Published in final edited form as:
Invest Ophthalmol Vis Sci. 2008 July ; 49(7): 3004–3017. doi:10.1167/iovs.07-1355.

Contribution of TRPV1 to Microglia-Derived IL-6 and NFκB Translocation with Elevated Hydrostatic Pressure

Rebecca M. Sappington and **David J. Calkins**
Department of Ophthalmology and Visual Sciences, Vanderbilt Eye Institute, Vanderbilt University Medical Center, Nashville, Tennessee.

Abstract

Purpose—The authors investigated the contributions of the transient receptor potential vanilloid-1 receptor (TRPV1) and Ca^{2+} to microglial IL-6 and nuclear factor kappa B (NFκB) translocation with elevated hydrostatic pressure.

Methods—The authors first examined IL-6 colocalization with the microglia marker Iba-1 in the DBA/2 mouse model of glaucoma to establish relevance. They isolated microglia from rat retina and maintained them at ambient or elevated (+70 mm Hg) hydrostatic pressure in vitro and used ELISA and immunocytochemistry to measure changes in the IL-6 concentration and NFκB translocation induced by the Ca^{2+} chelator EGTA, the broad-spectrum Ca^{2+} channel inhibitor ruthenium red, and the TRPV1 antagonist iodo-resiniferatoxin (I-RTX). They applied the Ca^{2+} dye Fluo-4 AM to measure changes in intracellular Ca^{2+} at elevated pressure induced by I-RTX and confirmed TRPV1 expression in microglia using PCR and immunocytochemistry.

Results—In DBA/2 retina, elevated intraocular pressure increased microglial IL-6 in the ganglion cell layer. Elevated hydrostatic pressure (24 hours) increased microglial IL-6 release, cytosolic NFκB, and NFκB translocation in vitro. These effects were reduced substantially by EGTA and ruthenium red. Antagonism of TRPV1 in microglia partially inhibited pressure-induced increases in IL-6 release and NFκB translocation. Brief elevated pressure (1 hour) induced a significant increase in microglial intracellular Ca^{2+} that was partially attenuated by TRPV1 antagonism.

Conclusions—Elevated pressure induces an influx of extracellular Ca^{2+} in retinal microglia that precedes the activation of NFκB and the subsequent production and release of IL-6 and is at least partially dependent on the activation of TRPV1 and other ruthenium red-sensitive channels.

Glaucoma is a common optic neuropathy characterized by progressive loss of retinal ganglion cells (RGCs) and is often associated with increases in intraocular pressure.[1–3] Although pathologic changes in the physiology of RGCs and their axons, which comprise the optic nerve, are primarily responsible for vision loss in glaucoma, other ocular cell types have also emerged as contributors to the disease process. In particular, astrocyte glia and

Corresponding author: David J. Calkins, Department of Ophthalmology and Visual Sciences, Vanderbilt Eye Institute, Vanderbilt University Medical Center, Ophthalmology Research Laboratory, 1105 Medical Research Building IV, Nashville, TN 37232-0654; david.j.calkins@vanderbilt.edu.

Disclosure: **R.M. Sappington**, None; **D.J. Calkins**, None

microglia have been associated with various aspects of glaucoma. These include biochemical and structural changes in the optic nerve head, vascular pathology, and direct modulation of RGC survival.[4–20] The contribution of glia to these events is often attributable to a change in the production or release of secreted factors. Increases in the level of inflammatory cytokines, such as tumor necrosis alpha (TNFα), interleukin (IL)-6, interferon gamma (IFNγ), IL-1α, IL-1β, IL-8, and IL-10, are evident in plasma and cerebral spinal fluid from a number of optic neuropathies, including neuromyelitis optica,[21] optic neuritis,[22] and AIDS-related optic neuropathy.[23] Similarly, levels of IL-6 in the aqueous humor of patients with neovascular glaucoma are markedly increased.[24] Growing evidence suggests that astrocyte glia and microglia produce these cytokines in glaucomatous optic neuropathy and AIDS-related optic neuropathy.[4,7,23] Experimental models using elevated pressure or ischemic conditions reveal that many extracellular factors, including TNFα,[4,5] nitric oxide,[6] and IL-6,[13,14,25,26] are released by astrocytes and microglia and can alter RGC survival.

We recently identified IL-6 as a key component of pressure-induced signals from retinal microglia and described its protective properties for RGCs exposed to elevated pressure.[13] We further identified the ubiquitin–proteasome pathway and activation of the transcription factor nuclear factor kappa B (NFκB), which are responsible for the production of IL-6 by astrocytes, microglia, and macrophages in other systems,[27–37] as components of the pressure-induced release of IL-6.[14] In other systems, the influx of extracellular Ca^{2+} can induce IL-6 production through the activation of NFκB,[38–41] including that induced by cellular stretch.[42] In microglia, Ca^{2+} mediates the response to a number of stimuli, including the activation of purinergic receptors, glutamate, and various proinflammatory cytokines.[43] Here, to probe its relevance to glaucoma, we found that microglia-derived IL-6 increases with elevated intraocular pressure (IOP) in the DBA/2 mouse model of hereditary glaucoma. To probe the mechanisms of IL-6 release in vitro, we describe the influence of Ca^{2+} chelation and of blocking Ca^{2+} channels on pressure-induced activation of NFκB and subsequent IL-6 release by retinal microglia. We also describe the novel finding that retinal microglia, like microglia in the brain and spinal cord,[44,45] express the capsaicin-sensitive, cation-selective transient receptor potential vanilloid-1 receptor (TRPV1). Using a hydrostatic pressure chamber, we determined that extracellular Ca^{2+} is required for pressure-induced IL-6 release and activation of NFκB in primary cultures of retinal microglia. Broad antagonism of ryanodine receptors and of TRPV1 with ruthenium red also inhibited IL-6 release and NFκB activation, though less efficiently. Specific antagonism of TRPV1 with iodo-resiniferatoxin (I-RTX; Alexis Biochemicals, Lausen, Switzerland) partially reduced the pressure-induced IL-6 release and activation of NFκB and the pressure-induced increases in intracellular Ca^{2+}. Interestingly, the activation of TRPV1 alone, with its agonist capsaicin, was not sufficient to increase IL-6 concentration. Together these data suggest that elevated hydrostatic pressure induces an influx of extracellular Ca^{2+} in retinal microglia that precedes the activation of NFκB and the subsequent production and release of IL-6. This influx is mediated in part by the activation of TRPV1, though other pressure-induced events are necessary to promote increases in IL-6 release.

MATERIALS AND METHODS

Animals and Tissue Preparation

This study was conducted in accordance with regulations set forth in the ARVO Statement for the Use of Animals in Ophthalmic and Vision Research. Animal protocols were approved by the Institutional Animal Care and Use Committee of the Vanderbilt University Medical Center. For DBA/2 studies, paraformaldehyde (4%)-fixed whole eyes from 6-month-old DBA/2 mice with relatively low (average, 14.7 mm Hg) or higher (average, 21.2 mm Hg) IOP were obtained from Philip Horner (University of Washington, Seattle, WA) and were prepared for immunolabeling as whole mount specimens. As previously described, IOP was monitored monthly with a tonometer (Tono-Pen; Reichert, Depew, NY) before kill.[46] For histology, adult Sprague–Dawley rats (Charles River Laboratories, Wilmington, MA) were perfused with 4% paraformaldehyde (Sigma, St. Louis, MO), their eyes were enucleated, and their retinas were removed for whole mount preparations. For primary cultures of purified microglia, eyes from postnatal day (P) 4 to P10 Sprague–Dawley rats (Charles River Laboratories) were enucleated, and retinas were dissected, as previously described.[13,14]

Cell Separation and Primary Culture

Primary cultures of purified retinal microglia were prepared as we previously described and published in this journal.[13,14] Briefly, retinas from P4 to P10 Sprague–Dawley rats were dissociated by trituration and incubation at 37°C in 1 mg/mL papain + 0.005% DNase I (Worthington, Lakewood, NJ). Viability was assessed by trypan blue exclusion. To purify microglia, the cells were incubated in monoclonal anti-rat RT 1a/OX18 antibody (5 μg/mL; catalog number CBL1519; Chemicon, Temecula, CA) or monoclonal anti-rat RT 1a/OX18 antibody (8 μg/mL; catalog number MCA51R; AbD Serotec, Raleigh, NC) followed by incubation with a magnetic bead-conjugated secondary antibody (Miltenyi Biotec, Auburn, CA). The cells were then loaded into a preequilibrated column in the presence of a magnetic field (Miltenyi Biotec). Cells positively selected by the anti-OX18 antibody were eluted, plated at a density of 5×10^4 on two-chamber glass slides or 1×10^4 on eight-chamber glass slides (Nalge-Nunc, Rochester, NY), and maintained in a 50:50 mixture of Dulbecco modified Eagle medium and F12 medium (DMEM/F12; Invitrogen, Carlsbad, CA) plus supplements. Cultures were grown to approximately 80% confluence (10–14 days) in a standard incubator with 5% CO_2 before our timed experiments. During this time, 50% of the culture media were replaced every 48 hours. As previously reported, the purity of our microglial cultures was determined by positive immunolabeling and PCR reactions for microglia-specific markers (OX18 and CD68) and by negative results for markers against astrocytes, Müller glia, and fibroblasts.[13] Cultures not meeting a standard of 95% purity were discarded.

Hydrostatic Pressure Experiments

We exposed microglia cultures to either ambient or +70 mm Hg hydrostatic pressure for 24 hours. This magnitude of pressure was chosen to complement our previous work; the rationale for using 70 mm Hg and construction of the pressure chamber is described in detail.[13,14] For elevated pressure, a humidified pressure chamber equipped with a regulator

and a gauge chamber was placed in a 37°C oven, and an air mixture of 95% air and 5% CO_2 was pumped into the chamber to obtain +70 mm Hg pressure that was maintained by the regulator. For ambient pressure experiments, cells were kept in a standard incubator. As described previously, pH and dissolved O_2 content were monitored experimentally to maintain values within the range for our ambient cultures.[14] For all pressure experiments, at least three culture plates per condition were used.

Pharmacology

Stock solutions of pharmacologic agents were diluted with microglia culture media to produce the following final concentrations: 950 μM ethylene glycol-bis(B-aminoethyl)-N,N,N^1,N^1-tetraacetic acid (EGTA; Invitrogen),[47] 0.7 μM, 7 μM, or 70 μM ruthenium red (Calbiochem, San Diego, CA), 0.1 μM, 1 μM, or 10 μM I-RTX (Alexis Biochemicals), and 1 μM capsaicin (Sigma).[48–50] Stock solutions were prepared as follows: 100 mM EGTA in NaOH-buffered ddH_2O, 10 mM ruthenium red in ddH_20, 10 mM I-RTX in dimethyl sulfoxide (DMSO), and 10 mM capsaicin in ethanol. Our calculations predict that 950 μM EGTA reduced the concentration of free Ca^{2+} in the media from 1 mM to 100 μM, as determined (Max Chelator; Stanford University, Stanford, CA). This dose was chosen to maximally chelate extracellular Ca^{2+} while avoiding the disruption of cell adhesion.[51–57] Control cultures for pharmacology studies were treated with an equivalent volume of the vehicle(s) sterile H_2O (EGTA and ruthenium red), DMSO (I-RTX), or ETOH (capsaicin).

Enzyme-Linked Immunoabsorbent Assay

We used ELISA to measure the concentration of IL-6 secreted by microglia in response to elevated pressure and capsaicin. The culture media were prepared for analysis, and ELISA assays were performed, as previously described.[13,14] Briefly, the media were first centrifuged at low speed to remove intact cells and were centrifuged again at a high speed to remove cellular debris. ELISA was conducted with anti-rat IL-6 ELISA kits (R&D Systems, Minneapolis, MN) according to manufacturer's recommendations. Each sample well was run in duplicate, thus providing six total measurements per condition. The concentration of IL-6 in each sample was determined by a comparison of the optical densities in the sample wells to that of the standard curve (Molecular Devices, Sunnyvale, CA). To determine the sensitivity of the IL-6 ELISA kit, we calculated the minimal concentration of cytokine necessary for detection. Based on the experimental optical density values, we performed a back calculation of cytokine concentration for the zero standards in 14 separate assays. These concentrations were averaged, and the standard deviation was multiplied by 2 to obtain a minimum reliable detection of 2.3983 pg/mL.

Calcium Signaling Experiments

To assess pressure-induced changes in intracellular Ca^{2+}, we used the Ca^{2+} dye Fluo-4 AM (Molecular Probes, Eugene, OR). This dye is closely related to Fluo-3, which has been used in many studies for live Ca^{2+} imaging and for measuring Ca^{2+} accumulation.[58–63] Fluo-4 is a BAPTA-based, nonratiometric Ca^{2+} dye that exhibits more than a 40-fold increase in fluorescence with Ca^{2+} binding.[64] Although changes in Ca^{2+} signaling are apparent within milliseconds for many stimuli, we were interested in longer changes in intracellular Ca^{2+} that could lead to a sustained cellular event, such as pressure-induced production and release

of IL-6 in retinal microglia.[14] Thus, we chose to examine Fluo-4 label after exposure to the stimulus for 1 hour, consistent with the period for reliable detection and interpretation of Fluo-4 label.[64] To allow complete de-esterification of Fluo-4 AM, primary microglia cultures were loaded with 5 μM Fluo-4 AM for 30 minutes in a standard culture incubator. The media were replaced, and the cultures were examined to confirm comparable Fluo-4 loading. When this was complete, the cultures were segregated into control and experimental groups. The experimental group was exposed to +70 mm Hg hydrostatic pressure in our specialized chamber for 1 hour, and the control group was maintained in a standard culture incubator. Immediately after the experiment, the live cultures were coverslipped with physiological saline and imaged on the microscope. For each sample, 15 to 20 independent fields (20×) were acquired, surface plots were created, and Fluo-4 intensity was quantified as total fluorescent intensity across the field.

Statistical Analysis

For comparison of ELISA data between treatment groups, we compared the mean concentration of IL-6 from a minimum of three separate experiments with the Student's *t*-test, where $P < 0.05$ was considered statistically significant. For comparison of Fluo-4 data between treatment groups, we compared the mean total intensity from a minimum of three separate experiments, which included 15 to 20 measurements each, with the Student's *t*-test, where $P < 0.05$ was considered statistically significant. All data are reported as mean ± SE.

Immunohistochemistry

For IL-6 and TRPV1 colocalization studies, immunolabeling in whole mount retina was performed as previously described, with the addition of heat-mediated antigen retrieval (10 mM citrate buffer, pH 6.0) for the microglial marker Iba-1.[13,14,65,66] For IL-6 studies, immunolabeling was performed with rabbit anti–IL-6 IgG (1:400; catalog number ab6672; Abcam, Cambridge MA) and goat anti-Iba-1 (1:400; catalog number ab5076; Abcam) and were visualized with donkey anti-rabbit IgG conjugated to an Alexa 488 fluorophore (10 μg/mL; Molecular Probes) and donkey anti-goat IgG conjugated to an Alexa 594 fluorophore (10 μg/mL; Molecular Probes). For TRPV1, immunolabeling was performed with rabbit anti-TRPV1 (1:100; catalog number NB100– 1617; Novus Biologicals, Littleton, CO) and mouse anti–Iba-1 (1 μg/mL; Abcam) and was visualized with goat anti-mouse IgG conjugated to an Alexa 594 fluorophore (10 μg/mL; Molecular Probes) and goat antirabbit IgG conjugated to an Alexa 488 fluorophore (10 μg/mL; Molecular Probes). Controls for immunohistochemistry experiments were conducted with no primary antibody and the appropriate IgG isotypes.

Immunocytochemistry

Immunolabeling in primary cultures of microglia cultures and whole mount preparations of rat retina was performed with slight modification, as previously described.[13,14,64,65] For NFκB translocation studies, immunolabeling was performed with mouse anti-NFκB p65 subunit (1 μg/mL; BD PharMingen, San Diego, CA) and was visualized with goat anti-mouse IgG conjugated with Alexa 488 fluorophore (10 μg/mL; Molecular Probes). Samples were also counterstained with the nuclear dye DAPI (50 μg/mL; Molecular Probes).

Controls for ICC experiments were conducted with no primary antibody and the appropriate IgG isotypes.

Fluorescence Microscopy

NFκB immunolabeling, TRPV1 immunolabeling, and Fluo-4 labeling in primary cultures of retinal microglia cultures were examined with an upright microscope equipped with differential interference contrast (DIC), a fluorescent lamp, and four wavelength cubes (Olympus, Melville, NY) digitally interfaced with semicooled charge-coupled device cameras and image capture software (Diagnostic Instruments, Sterling Heights, MI). Imaging of immunolabeling in whole mount retina against IL-6 + Iba-1 and TRPV1 + Iba-1 was performed at the Vanderbilt Cell Imaging Core on an upright confocal microscope (LSM510 META; Zeiss, Thornwood, NY) equipped with laser scanning fluorescence (blue/green, green/red, red/far-red) and Nomarski-DIC, 3-D z-series, and time-series. All samples were examined with a 63× oil-immersion objective (1.40; Plan-Apochromat; Zeiss), and images were acquired with a digital camera (AxioCam HR; Zeiss) and image analysis software (LSM 5; Zeiss).

Reverse Transcription–Polymerase Chain Reaction

Total RNA was isolated, according to the manufacturer's instructions, from isolated microglia and whole retina using extraction kits (MicroRNA and RNeasy; Qiagen, Inc., Valencia, CA). RT-PCR was performed as previously described.[13,14] After first- and second-strand synthesis of cDNA, gene-specific PCR was conducted for 30 cycles with primers against rat *trpv1* that were designed to span an intron (Integrated DNA Technologies, Coralville, IA): 5′-CAA GCA CTC GAG ATA GAC ATG CCA-3′ and 5′-ACA TCT CAA TTC CCA CAC ACC TCC-3′. The resultant PCR product of 282 bp was separated on an agarose gel stained with ethidium bromide and digitally imaged on a gel reader (Alpha Innotech, San Leandro, CA). To ensure that resultant bands were not the product of contamination with genomic DNA, gene-specific PCR without reverse transcription was performed on RNA samples from each culture.

RESULTS

Microglia-Derived IL-6 in the DBA/2 Mouse Model of Glaucoma

We have previously shown that primary cultures of purified microglia increase the production and release of IL-6 in response to elevated hydrostatic pressure.[13,14] This microglia-derived IL-6 can increase the survival of RGCs also exposed to elevated hydrostatic pressure.[13] To test whether microglia-derived IL-6 could be relevant in vivo, we examined the colocalization of IL-6 and the microglia marker Iba-1 in whole mount preparations of retina from 6-month-old DBA/2 mice with relatively low IOP (average, 14.7 mm Hg) and higher IOP (average, 21.2 mm Hg). The DBA/2 mouse is a model of pigmentary glaucoma in which iris stromal atrophy and iris pigment dispersion, caused by mutations in the *Tyrp1* and *Gpnmb* genes, lead to elevated IOP that rises significantly across the population between 6 and 9 months of age.[67,68] In DBA/2 mice with relatively low IOP, IL-6 was present at levels just detectable in the extracellular space within the ganglion cell layer (Fig. 1A), and Iba-1 labeling identified the presence of microglia in the same plane

(Fig. 1B). A direct comparison of the two markers revealed IL-6 within microglia cell bodies and processes (Fig. 1C); this is shown at higher magnification in Figure 1G. In contrast, retinas from DBA/2 mice with higher IOP demonstrated marked increases in labeling for IL-6 in the ganglion cell layer (Fig. 1D), again especially in the extracellular space surrounding RGCs and in what appeared to be microglial processes. This was confirmed with labeling against Iba-1 (Fig. 1E), which also revealed hypertrophy and increased ramification of microglia. A direct comparison of IL-6 and Iba-1 showed strong colocalization (Fig. 1F) that was even more apparent at high magnification (Fig. 1H), suggesting that microglia are a source of the elevated extracellular IL-6. We also noted IL-6 labeling in cells on the superficial surface of the nerve fiber layer (data not shown); these exhibited morphology consistent with astrocytes, suggesting another source of IL-6. Together, these data confirm that elevated IOP, like elevated hydrostatic pressure, increases microglial IL-6. Furthermore, the presence of IL-6 in the extracellular space surrounding RGCs suggests that RGCs are a likely target for an IL-6 signal.

Pressure-Induced IL-6 Release, NFκB Translocation, and Extracellular Ca^{2+}

To continue our examination of mechanisms that underlie the pressure-induced production and release of IL-6 by microglia, we tested whether extracellular Ca^{2+} contributes to the pressure-induced release of IL-6 from retinal microglia, as it does in other cells.[38–41] We maintained isolated microglia for 24 hours at either ambient or +70 mm Hg hydrostatic pressure after chelation of extracellular Ca^{2+} with 950 μM EGTA, which reduced the concentration of free Ca^{2+} in the media from 1 mM to 100 μM (see Materials and Methods). We then measured the concentration of IL-6 in the culture media using ELISA. Consistent with our previous findings,[13,14] IL-6 secretion from microglia at ambient pressure was relatively low (135 ± 7.5 pg/mL; Fig. 2). Treatment with EGTA slightly increased the concentration of IL-6 to 196 ± 9.4 pg/mL, a significant departure from ambient pressure alone ($P = 0.02$; Fig. 2). Also consistent with our previous findings, exposure to elevated pressure induced an almost 10-fold increase in IL-6 concentration compared with ambient pressure (1276 ± 51.9 pg/mL; $P \ll 0.01$; Fig. 2). This pressure-induced increase was reduced by 66% after Ca^{2+} chelation by EGTA (430 ± 9.4 pg/mL), though even this level of IL-6 was threefold greater than that observed at ambient pressure alone ($P \ll 0.01$; Fig. 2). These data suggest that extracellular Ca^{2+} has a different effect on IL-6 release, depending on pressure, slightly attenuating IL-6 release at ambient pressure while promoting IL-6 release in response to elevated pressure.

Pressure-induced microglial release of IL-6, like that of IL-6 induced by other stimuli,[27–37] arises significantly from de novo synthesis mediated by upstream activation of the transcription factor NFκB.[14] This activation is early and sustained; translocation is evident within 8 hours of exposure and is maintained for more than 72 hours.[14] To determine whether the observed effects of chelating extracellular Ca^{2+} on IL-6 release could arise by modulation of this transcriptional event, we examined the nuclear translocation of NFκB after the same exposure to elevated pressure, again in the presence or absence of EGTA. Consistent with our published results, at ambient pressure NFκB in microglia was localized exclusively to the cytosol, as determined by comparing p65 immunolabeling for NFκB with the nuclear counterstain DAPI (Fig. 3A). Chelation of extracellular Ca^{2+} with EGTA at

ambient pressure induced a minute increase in nuclear labeling of NFκB (Fig. 3B). This should be compared with the slight increase in IL-6 at ambient pressure with EGTA, as measured by ELISA (Fig. 2).

Consistent with our earlier findings, exposure to elevated pressure increased the intensity of cytosolic labeling and also induced significant translocation to the nucleus (Fig. 3C). In contrast, Ca^{2+} chelation with EGTA at elevated pressure significantly decreased the intensity of nuclear labeling and overall cytosolic levels of NFκB (Fig. 3D). Treatment with EGTA appeared to have qualitatively altered the shape of nuclei in our microglia cultures. However, an analysis of nuclei size revealed no statistical difference between the treatment groups (data not shown). These results suggest that, like IL-6 release, extracellular Ca^{2+} could differentially regulate the translocation of NFκB, depending on pressure, promoting translocation at elevated pressure (compare Figs. 3C and 3D) while potentially attenuating translocation at ambient pressure (compare Figs. 3A and 3B).

Pressure-Induced IL-6 Release, NFκB Translocation, and Ca^{2+} Channels

To begin the task of identifying Ca^{2+} channels that may contribute to the Ca^{2+}-dependent release of IL-6 and the translocation of NFκB, we maintained microglia at ambient or elevated pressure for 24 hours in the presence or absence of the broad-spectrum Ca^{2+} channel antagonist ruthenium red (0.7–70 μM) and again assessed IL-6 with ELISA and translocation of NFκB with immunocytochemical labeling. We chose ruthenium red (IC_{50}, 7 μM) as our initial antagonist because of its ability to inhibit ryanodine-sensitive channels and TRPV1,[69–75] which are both reported to modulate Ca^{2+} activity in microglia.[44,76,77]

In microglia cultures maintained at ambient pressure, treatment with ruthenium red did not significantly alter the basal concentration of IL-6 in the culture media ($P > 0.05$ for all; Fig. 4). In contrast, ruthenium red altered the pressure-induced release of IL-6 in a dose-dependent manner. At our lowest concentration (0.7 μM), ruthenium red actually increased the concentration of IL-6 in the culture media at elevated pressure by 22% (1647 ± 157.8 pg/ml) compared with elevated pressure alone ($P < 0.01$; Fig. 4). This increase was reversed at the median IC_{50} concentration (7 μM) and at the highest concentration (70 μM), which decreased IL-6 concentrations at elevated pressure by 28% (920 ± 106.3 pg/ml; $P < 0.01$) and 37% (804 ± 143 pg/ml; $P \ll 0.01$), respectively (Fig. 4). These data suggest that the pressure-induced release of IL-6 by retinal microglia is at least partially regulated by Ca^{2+} flux through channels sensitive to ruthenium red.

As in the IL-6 studies, treatment with ruthenium red at all concentrations did not alter the levels or localization of NFκB at ambient pressure, which was almost exclusively cytosolic (Figs. 5A–D). Like IL-6 release, the effects of ruthenium red on the translocation of NFκB at elevated pressure were dose dependent. In agreement with the observed effect on IL-6 release (Fig. 4), treatment with 0.7 μM ruthenium red did not significantly change pressure-induced translocation of NFκB to the nucleus (compare Figs. 5E and 5F). In contrast, treatment with 7 μM (Fig. 5G) and 70 μM ruthenium red (Fig. 5H) greatly diminished the translocation of NFκB, as seen by decreased colocalization of p65 label with the DAPI nuclear stain. These concentrations were also accompanied by a decrease in the intensity of cytosolic labeling of NFκB, compared with treatment with 0.7 μM ruthenium red (Fig. 5F).

These data suggest that, like the Ca^{2+}-dependent release of IL-6, nuclear translocation of NFκB in response to elevated pressure is mediated by Ca^{2+} channels sensitive to ruthenium red. Interestingly, these channels do not appear to regulate the basal release of IL-6 or the translocation of NFκB, as suggested by the absence of a response to ruthenium red in cultures maintained at ambient pressure (Figs. 4, 5A–D).

Pressure-Induced Release of IL-6, Translocation of NFκB, and TRPV1 Antagonism

Results in Figures 2 and 3 demonstrate that the chelation of extracellular Ca^{2+} dramatically reduced IL-6 release and NFκB translocation. These data suggest that Ca^{2+} influx from the extracellular milieu is a likely contributor to pressure-induced effects. Ruthenium red, which inhibits TRPV1 and ryanodine receptors,[69–75] also attenuated pressure-induced IL-6 release and NFκB translocation (Figs. 4, 5). Although TRPV1 is associated with the influx of extracellular Ca^{2+} and the release of Ca^{2+} from intracellular stores, ryanodine receptors are exclusively associated with the release of Ca^{2+} from intracellular stores.[78,79] Thus, we focused next on the potential contribution of TRPV1 to the pressure-induced release of IL-6 and translocation of NFκB.

We exposed primary cultures of retinal microglia to ambient or elevated pressure for 24 hours in the presence of the TRPV1-specific antagonist iodo-resiniferatoxin (I-RTX; 0.1–10 μM). Again, we measured the concentration of IL-6 in the culture media and examined the immunolabeling of p65 NFμB. The median dose of 1 μM was selected from extensive literature in which this dose reliably inhibited TRPV1-dependent behaviors across multiple systems.[80–83] At ambient pressure, treatment with I-RTX did not significantly alter the concentration of IL-6 in the media ($P > 0.05$ for all; Fig. 6A). In contrast, for microglia exposed to elevated pressure, treatment with I-RTX reduced the concentration of IL-6 in the media. This effect was dose dependent, where the lowest concentration of I-RTX (0.1 μM) did not significantly alter the concentration of IL-6 (1196 ± 61.3 pg/ml; $P = 0.41$), and the median and highest doses (1 μM and 10 μM) reduced the media concentration of IL-6 by 25% (954 ± 77.7 pg/ml; $P < 0.01$) and 26% (939 ± 100 pg/ml; $P < 0.01$), respectively (Fig. 6A). However, it is important to note that I-RTX did not reduce the concentration of IL-6 to levels observed at ambient pressure. In fact, IL-6 levels remained sevenfold higher than levels at ambient pressure ($P \ll 0.01$ for both; Fig. 6A). Consistent with this observation, the pharmacologic activation of TRPV1 with 1 μM capsaicin, a well-established dose for activating TRPV1,[84–88] did not alter the concentration of IL-6 in the culture media (Fig. 6B). These data suggest that TRPV1 antagonism induces partial inhibition of pressure-induced increases in IL-6 release by microglia. However, the activation of TRPV1 alone is not sufficient to promote IL-6 release.

Despite the moderate effect of I-RTX on pressure-induced increases in the media concentration of IL-6, treatment with I-RTX greatly diminished pressure-induced translocation of NFκB to the nucleus. Consistent with our analysis of IL-6, I-RTX did not appear to alter the pattern of NFκB in cultures maintained at ambient pressure, where NFκB was almost exclusively restricted to the cytosol (Figs. 7A–D). In contrast, the effects of I-RTX on pressure-induced translocation of NFκB and increased cytosolic levels (Fig. 7E) were dose dependent. The 0.1-μM dose of I-RTX slightly reduced the colocalization of

NFκB with DAPI, particularly in the center of the nucleus (Fig. 7F). Cytosolic levels were also slightly diminished. The trend toward reduced NFκB translocation and cytosolic levels continued with the median and highest doses of I-RTX (Figs. 7G, 7H), where the 10-μM dose demonstrated the most pronounced separation of p65 label and DAPI (Fig. 7H). Similar to labeling with the highest dose of ruthenium red, the 10-μM dose of I-RTX also reduced most dramatically the intensity of NFκB in the cytosol (compare Figs. 7H and 5H). These data suggest that the antagonism of TRPV1 significantly diminishes the activation and translocation of NFκB in retinal microglia exposed to elevated pressure. Interestingly, the effect of I-RTX on NFκB translocation was far more striking than that observed on levels of IL-6 in media, suggesting that TRPV1 activity may have a greater impact on early signaling events related to the initiation of IL-6 transcription rather than on the actual release of the signaling molecule.

Elevated Pressure and Microglial Intracellular Ca^{2+}

Figure 2 indicates that the chelation of extracellular Ca^{2+} inhibits the pressure-induced release of IL-6 and the translocation of NFκB, implying that each requires an increase in intracellular Ca^{2+} through influx from the extracellular domain. To determine whether elevated pressure increases intracellular Ca^{2+} in microglia and whether TRPV1 contributes directly to these increases, we measured pressure-induced changes in Fluo-4 AM fluorescence as an indicator of changes in cytosolic Ca^{2+}. We examined the localization and intensity of Fluo-4 label in microglia cultures exposed to ambient or elevated pressure for 1 hour in the presence of I-RTX (1 μM). Fluo-4 label in microglia maintained at ambient pressure was low and was restricted to the cell body (Fig. 8A). Exposure to elevated pressure for 1 hour dramatically increased Fluo-4 label in microglia cell bodies and induced an expansion of signal to include processes (Fig. 8B). These differences are readily apparent by comparing the surface rendering of the Fluo-4 signal at ambient pressure with that representing elevated pressure (Figs. 8A, 8B). Specific antagonism of TRPV1 with 1 μM I-RTX greatly reversed most of the pressure-induced increases in Fluo-4 label, particularly in microglial processes (compare Figs. 8C and 8B). In contrast, treatment with I-RTX did not appear to affect the distribution of Fluo-4 label in microglia maintained at ambient pressure (Fig. 8D). Quantification of total signal intensity revealed an overall twofold increase in microglia Ca^{2+} with elevated pressure compared with ambient pressure ($P < 0.01$; Fig. 8E). This pressure-induced increase was reduced by 26% after treatment with I-RTX ($P < 0.01$; Fig. 8E). However, treatment with I-RTX did not reduce Fluo-4 levels to those observed at ambient pressure ($P = 0.02$; Fig. 8E). In contrast, treatment with I-RTX did not alter Fluo-4 label in microglia maintained at ambient pressure ($P = 0.47$; Fig. 8E). These data suggest that the increases in intracellular Ca^{2+} in retinal microglia caused by exposure to elevated pressure are prolonged in terms of Ca^{2+} signaling but far precede the pressure-induced translocation of NFκB and increased IL-6 release. Furthermore, these increases arise in part by the activation of TRPV1.

Expression of TRPV1 in Retinal Microglia

Finally, we examined the expression of TRPV1 in our microglia cultures and the localization of TRPV1 to microglia of the adult rat retina in situ. TRPV1 in microglia cultures is diffusely distributed throughout the cell body and cellular processes (Fig. 9A).

The presence of perinuclear label and the diffuse nature of somal labeling suggests that TRPV1 is most likely present in the endoplasmic reticulum and on the plasma membrane (Fig. 9A).[89,90]

Coimmunolabeling of TRPV1 and the microglia-specific marker Iba-1 in whole mount preparations of the retina from adult rat reveals the presence of TRPV1 on the cell body and processes of microglia near the nerve fiber layer, as determined by confocal microscopy (Fig. 9B). The punctate nature of TRPV1 labeling suggests plasma membrane expression of TRPV1. However, TRPV1 may also be present in the membranes of the endoplasmic reticulum.[89,90] Together with our analysis of IL-6 release and NFκB translocation, these data suggest that TRPV1 is a viable candidate for further assessment of the contribution to Ca^{2+}-dependent IL-6 release and NFκB translocation in microglia exposed to elevated pressure.

DISCUSSION

Our previous work demonstrated that retinal microglia in vitro increase the release of IL-6 in response to elevated hydrostatic pressure and that this increase in IL-6 affords protection against pressure-induced apoptosis in RGCs.[13,14] Here we provide evidence that microglia-derived IL-6 is a component of IOPrelated changes in the DBA/2 retina. We demonstrate that as IOP increases, IL-6 is present at significantly higher levels in the extracellular space surrounding RGCs and within the processes of highly ramified microglia (Fig. 1). Our data suggest that, like elevated hydrostatic pressure, elevated IOP is a stimulus for IL-6 production in microglia in vivo. Furthermore, it is likely that microglia, with both relatively low and relatively high IOP, are a source of the extracellular IL-6 in retina. Together these data validate the potential significance of microglia-derived IL-6 on RGC survival in glaucoma, as suggested by our previous studies.[13,14]

Mechanistically, we also previously demonstrated that the activation of retinal microglia by elevated hydrostatic pressure involves the activation of NFκB and the subsequent production and release of IL-6.[13,14] It is known that Ca^{2+} and Ca^{2+} channels mediate the activation of microglia in response to a number of stimuli, such as activated purinergic receptors, glutamate, and various proinflammatory cytokines.[43] Here we determined that Ca^{2+} is a strong modulator of pressure-induced IL-6 release and NFκB translocation. By chelating extracellular Ca^{2+} with EGTA, we determined that Ca^{2+} plays a role in promoting IL-6 release and NFκB translocation in response to pressure but could attenuate IL-6 and NFκB translocation under ambient conditions (Figs. 2, 3). Interestingly, the effect of Ca^{2+} chelation on the translocation of NFκB appears less significant than that observed with IL-6 release. Furthermore, it is important to note that our dose of EGTA did not reduce IL-6 levels to those measured at ambient pressure. Although a larger dose of EGTA would likely reduce IL-6 levels further, data obtained from such a decrease in available Ca^{2+} could not be interpreted as the result of a specific pathway. Instead, these data would likely have stemmed from global responses to prolonged deficiency in Ca^{2+} (i.e., decreased cell adhesion, inhibition of transcription, and cell death).[51–57] These data suggest that Ca^{2+} is involved in transcriptional and posttranscriptional events induced by elevated pressure. Although Ca^{2+} is likely to modulate pressure-induced release indirectly through the

induction of NFκB translocation, it appears to play a larger role in the direct induction of IL-6. These direct effects could occur at multiple levels of the signaling cascade, including translation, protein trafficking, and release mechanisms. Our data here do not distinguish among these cellular activities, but we are examining them in detail.

Many types of Ca^{2+} channels and transporters are responsible for the regulation of Ca^{2+} signaling. In microglia, ryanodine-sensitive channels and TRPV1 are reported to modulate Ca^{2+} activity that leads to various cellular responses.[44,77] Using ruthenium red, we examined the contribution of these two subsets of channels to the pressure-induced release of IL-6 and NFκB translocation (Figs. 4, 5). At elevated pressure, treatment with ruthenium red decreased IL-6 release and NFκB translocation at the two highest doses, suggesting that ryanodine-sensitive or TRPV1 channels are involved in regulating Ca^{2+}-dependent release of IL-6 and nuclear translocation of NFκB. Interestingly, the lowest dose of ruthenium red (0.7 μM) actually increased pressure-induced IL-6 release and NFκB translocation. Although the exact mechanism of this dose effect is unclear, it is likely that this effect stems from ruthenium red-induced inhibition of ryanodine-sensitive channels, which are competitively bound by ruthenium red at a dose as low as 0.3 μM.[91,92] In contrast to its effects on ryanodine-sensitive channels, ruthenium red is reported to attenuate TRPV1 through noncompetitive binding at doses ranging from 1 μM to 100 μM.[93–96] Although the involvement of ruthenium red-sensitive channels in pressure-induced effects is complex, these channels do not appear to modulate the basal release of IL-6 because ruthenium red did not alter IL-6 concentrations or NFκB translocation at ambient pressure.

We further examined the contribution of TRPV1 to pressure-induced IL-6 release and NFκB translocation (Figs. 6, 7). We determined that pharmacologic antagonism of TRPV1 with I-RTX attenuated the pressure-induced release of IL-6, but only by approximately 25%. Of note, the lowest dose of I-RTX did not alter IL-6 concentrations, whereas 1 μM and 10 μM I-RTX lowered IL-6 to almost identical levels (25% and 26%, respectively). A possible explanation for this ceiling effect is that the total contribution of TRPV1 translates to a 25% increase in IL-6 release at elevated pressure, so that 1 μM I-RTX may be sufficient to inhibit this contribution of TRPV1. However, the ability of 1 μM and 10 μM I-RTX to inhibit the translocation of NFκB suggests that TRPV1 activity contributes to early signaling events related to the initiation of IL-6 transcription. These data suggest that TRPV1 in microglia, like cells of the cornea, lung, and epidermis, can modulate the stimulus-induced production of proinflammatory cytokines, including IL-6.[97–99] However, the inability of I-RTX or ruthenium red to abolish pressure-induced increases in IL-6 release suggests that other cellular mechanisms contribute significantly to the IL-6 response. Furthermore, the fact that these antagonists had a greater effect on NFκB translocation than IL-6 release suggests these other mechanisms likely regulate IL-6 release at the protein rather than the transcriptional level.

Although TRP channels, including TRPV1, are activated by a wide range of stimuli, they are universally characterized by a strong Ca^{2+} conductance.[100–111] To verify that exposure to elevated hydrostatic pressure induced Ca^{2+} conductance through TRPV1 in retinal microglia, we measured changes in the intracellular intensity of the Ca^{2+} dye Fluo-4 AM in microglia exposed to elevated pressure (Fig. 8). Our examination of Fluo-4 labeling revealed

a global twofold increase in intensity over ambient levels. However, spatial mapping of Fluo-4 label revealed that the most dramatic change in Fluo-4 label occurred in microglial processes, which become more complex after exposure to elevated pressure in vivo.[112,113] In fact, the antagonism of TRPV1 with I-RTX, which reduced Fluo-4 intensity by 26%, had the greatest impact on labeling in the processes. Consistent with the IL-6 and NFκB data, I-RTX did not reduce Fluo-4 intensity at elevated pressure to ambient levels, suggesting the involvement of other Ca^{2+} channels in pressure-induced changes. Although the Fluo-4 data present clear evidence for increased Ca^{2+} resulting from exposure to elevated pressure, Fluo-4 does not differentiate between Ca^{2+} released from intracellular stores and Ca^{2+} influx from extracellular sources. However, chelation of extracellular Ca^{2+} with EGTA provided the most dramatic effect on IL-6 release, suggesting that the influx of extracellular Ca^{2+} is likely to contribute significantly to increases in Ca^{2+}. Of note, TRPV1-mediated increases in Fluo-4 label were evident after exposure to only 1 hour of elevated pressure. This was 7 hours before our previous observation of initial changes in IL-6 release and NFκB translocation.[14] Like pressure-induced IL-6 release, pressure-induced elevation in Ca^{2+} was only modestly attenuated by the antagonism of TRPV1. Together with the observed effect of Ca^{2+} chelation and Ca^{2+} channel blockers on IL-6 release and NFκB translocation and our earlier findings, these data suggest Ca^{2+} influx through TRPV1 may modulate pressure-induced IL-6 release and NFκB translocation. However, other mechanisms, which may also be Ca^{2+} dependent, play a significant role in these events. This is particularly likely at the protein level, where chelation and channel antagonism had the smallest impact on pressure-induced effects.

We should note here that the use of separate cultures for the measurement of Fluo-4 label at conditions of ambient and elevated pressure raises some possibilities for artifact. Specifically, no internal control is present for initial dye loading or dye leakage over time. We attempted to minimize these artifacts, while still using a high-affinity Ca^{2+} dye, in a number of ways. First, we examined each culture for equivalent dye loading before the start of the experiment. Any culture that did demonstrate qualitatively equivalent loading was excluded. Second, we used at least three and up to six culture plates per condition, for which the mean Fluo-4 intensity was determined and used in statistical comparisons. As such, a bias in dye loading that was not qualitatively identified would have to occur simultaneously in as many as six cultures. Similarly, our data required that the cultures maintained at elevated pressure had significantly slower rates of dye leakage than the cultures maintained at ambient pressure. For such an event to occur, elevated pressure must induce a statistically significant change in the membrane physiology of microglia compared with ambient pressure. Although we cannot rule out this possibility, the ability of I-RTX to reduce Fluo-4 signal at elevated pressure suggests that pressure-induced increases in Fluo-4 signal are the result of increased cytoplasmic Ca^{2+} rather than Fluo-4 retention.

In culture, TRPV1 was localized to processes and cell bodies, with evidence of perinuclear localization (Fig. 9). In adult retina, punctate immunolabel against TRPV1 was present in the processes of Iba-1–positive microglia (Fig. 9). The cell bodies of these microglia also exhibited diffuse labeling for TRPV1. As described in other tissues, TRPV1 can be localized to the plasma membrane and the endoplasmic reticulum.[89,90,114] The punctate labeling observed in microglial processes is consistent with localization to the plasma membrane.

However, the more diffuse labeling in the cell body may also indicate localization to the endoplasmic reticulum. Therefore, these data support a potential role for TRPV1 in the influx of extracellular Ca^{2+} and its release from intracellular stores. Although these data do not shed light on the source of TRPV1-mediated Ca^{2+} modulation in response to elevated pressure, they do establish the viability of TRPV1 as a contributor to the responses of microglia in vivo.

Although culture systems have many advantages for the analysis of many biological functions, including cell-type specific analysis of cytokine release, there is no doubt that these systems also present limitations and confounding factors. In our study, the biomechanics of exposure to regulated hydrostatic pressure in vitro differs greatly from those involved in chronic, progressive exposure to variations in elevated ocular pressure in vivo. In addition, we cannot rule out the possibility that IL-6 production at elevated pressure is in response to other signaling factors, including IL-1α, IL-1B, TNFα, and IFNγ,[115] rather than a direct response to elevated pressure. To produce a pressure stimulus that would be relevant to pressure stimuli in vivo, we based the design of our pressure chamber on those used to study the effect of hydrostatic pressure on cellular proliferation and membrane elasticity.[116] In our studies, we carefully controlled pH and temperature and have also examined the dissolved O_2 and CO_2 content of the media.[13,14] Others have shown that, when these factors are controlled or made negligible, the most likely sources of cellular perturbation are distortional strain, compression, and the gradient of liquid potential across the cell membrane.[6,117–119] Which of these cellular events lead to IL-6 production and NFκB translocation is unclear. However, it is likely that RGCs in vivo, particularly axons in the lamina cribosa, are likely to undergo similar strain and stretch in response to elevated IOP. Although the possibility remains that IL-6 is induced by other signaling factors rather than directly by pressure, the mechanistic components of the IL-6 pathway described in this study are active during exposure to elevated, but not ambient, pressure and lead to IL-6 release regardless of the exact nature of their induction.

In combination with our previous work, this study identifies Ca^{2+} and TRPV1 as components of a signaling pathway that leads to pressure-induced release of IL-6 by microglia. Our data demonstrate that Ca^{2+} modulation in response to elevated pressure occurs upstream of NFκB translocation and subsequent IL-6 production and release by retinal microglia. Furthermore, this Ca^{2+} modulation occurs in part through the cation channel TRPV1. Although TRPV1 does not account for the entire Ca^{2+} dependence of this signaling cascade, our data suggest that the contribution of TRPV1 is significant enough to inhibit the IL-6 response by approximately 25%. The identification of TRPV1 as a component of pressure-induced signaling distinguishes parallels between the pressure responses in retinal microglia and microglial activation in the brain and the stimulus-induced production of proinflammatory cytokines in other cell types.[97–100]

Acknowledgments

The authors thank Philip Horner (University of Washington, Seattle, WA) for DBA/2 mouse tissue, Brian J. Carlson (Vanderbilt University Medical Center, Nashville, TN), and the Cell Imaging Core (Vanderbilt University Medical Center, Nashville, TN) for technical assistance.

Supported by the Catalyst for a Cure Consortium (RMS, DJC) sponsored by the Glaucoma Research Foundation; a Challenge Grant and a Wasserman Award from Research to Prevent Blindness, Inc. (DJC); National Eye Institute Core Grant 5P30EY008126-19; and a grant from Fight for Sight, Inc. (RMS).

References

1. Hitchings, RA. What is primary open angle glaucoma?. In: Hitchings, RA., editor. Fundamentals of Clinical Ophthalmology: Glaucoma. London: BMJ Publishing Group; 2000. p. 1-8.
2. Jonas JB, Budde WM. Diagnosis and pathogenesis of glaucomatous optic neuropathy: morphological aspects. Prog Retinal Eye Res. 2000; 19:1–40.
3. Guo L, Moss SE, Alexander RA, Ali RR, Fitzke FW, Cordeiro MF. Retinal ganglion cell apoptosis in glaucoma is related to intraocular pressure and IOP-induced effects on extracellular matrix. Invest Ophthalmol Vis Sci. 2005; 46:175–182. [PubMed: 15623771]
4. Yuan L, Neufeld AH. Tumor necrosis factor-alpha: a potentially neurodestructive cytokine produced by glia in the human glaucomatous optic nerve head. Glia. 2000; 32:42–50. [PubMed: 10975909]
5. Tezel G, Wax MB. Increased production of tumor necrosis factor-α by glial cells exposed to simulated ischemia or elevated hydrostatic pressure induces apoptosis in cocultured retinal ganglion cells. J Neurosci. 2000; 20:8693–8700. [PubMed: 11102475]
6. Liu B, Neufeld AH. Nitric oxide synthase-2 in human optic nerve head astrocytes induced by elevated pressure in vitro. Arch Ophthalmol. 2001; 119:240–245. [PubMed: 11176986]
7. Tezel G, Li LY, Patil RV, Wax MB. TNF-α and TNF-α receptor-1 in the retina of normal and glaucomatous eyes. Invest Ophthalmol Vis Sci. 2001; 42:1787–1794. [PubMed: 11431443]
8. Agapova OA, Ricard CS, Salvador-Silva M, Hernandez MR. Expression of matrix metalloproteinases and tissue inhibitors of metalloproteinases in human optic nerve head astrocytes. Glia. 2001; 33:205–216. [PubMed: 11241738]
9. Agapova OA, Kaufman PL, Lucarelli MJ, Gabelt BT, Hernandez MR. Differential expression of matrix metalloproteinases in monkey eyes with experimental glaucoma or optic nerve transection. Brain Res. 2003; 967:132–143. [PubMed: 12650974]
10. Agapova OA, Yang P, Wang WH, et al. Altered expression of 3 alpha-hydroxysteroid dehydrogenases in human glaucomatous optic nerve head astrocytes. Neurobiol Dis. 2003; 14:63–73. [PubMed: 13678667]
11. Fuchs C, Forster V, Balse E, Sahel JA, Picaud S, Tessier LH. Retinal-cell-conditioned medium prevents TNF-alpha-induced apoptosis of purified ganglion cells. Invest Ophthalmol Vis Sci. 2005; 46:2983–2991. [PubMed: 16043875]
12. Agapova OA, Kaufman PL, Hernandez MR. Androgen receptor and NFkB expression in human normal and glaucomatous optic nerve head astrocytes in vitro and in experimental glaucoma. Exp Eye Res. 2006; 82:1053–1059. [PubMed: 16310187]
13. Sappington RM, Chan M, Calkins DJ. Interleukin-6 protects retinal ganglion cells from pressure-induced death. Invest Ophthalmol Vis Sci. 2006; 47:2932–2942. [PubMed: 16799036]
14. Sappington RM, Calkins DJ. Elevated pressure induces proteosome-dependent secretion of IL-6 and activation of NFκB in retinal glial cells. Invest Ophthalmol Vis Sci. 2006; 47:3860–3869. [PubMed: 16936098]
15. Inman DM, Horner PJ. Reactive nonproliferative gliosis predominates in a chronic mouse model of glaucoma. Glia. 2007; 55:942–953. [PubMed: 17457855]
16. Urban Z, Agapova O, Hucthagowder V, Yang P, Starcher BC, Hernandez MR. Population differences in elastin maturation in optic nerve head tissue and astrocytes. Invest Ophthalmol Vis Sci. 2007; 48:3209–3215. [PubMed: 17591890]
17. Grieshaber MC, Orgul S, Schoetzau A, Flammer J. Relationship between retinal glial cell activation in glaucoma and vascular dysregulation. J Glaucoma. 2007; 16:215–219. [PubMed: 17473733]
18. Malone P, Miao H, Parker A, Juarez S, Hernandez MR. Pressure induces loss of gap junction communication and redistribution of connexin 43 in astrocytes. Glia. 2007; 55:1085–1098. [PubMed: 17551925]

19. Malone PE, Hernandez MR. 4-Hydroxynonenal, a product of oxidative stress, leads to an antioxidant response in optic nerve head astrocytes. Exp Eye Res. 2007; 84:444–454. [PubMed: 17173895]
20. Tezel G, Yang X, Luo C, Peng Y, Sun SL, Sun D. Mechanisms of immune system activation in glaucoma: oxidative stress-stimulated antigen presentation by the retina and optic nerve head glia. Invest Ophthalmol Vis Sci. 2007; 48:705–714. [PubMed: 17251469]
21. Correale J, Fiol M. Activation of humoral immunity and eosinophils in neuromyelitis optica. Neurology. 2004; 63:2363–2370. [PubMed: 15623701]
22. Deckert-Schlüter M, Schlüter D, Schwendemann G. Evaluation of IL-2, sIL2R, IL-6, TNF-alpha, and IL-1 beta levels in serum and CSF of patients with optic neuritis. J Neurol Sci. 1992; 113:50–54. [PubMed: 1469455]
23. Saadati HG, Khan IA, Lin XH, Kadakia AB, Heller KB, Sadun AA. Immunolocalization of IL-1beta and IL-6 in optic nerves of patients with AIDS. Curr Eye Res. 1999; 19:264–268. [PubMed: 10487966]
24. Chen KH, Wu CC, Roy S, Lee SM, Liu JH. Increased interleukin-6 in aqueous humor of neovascular glaucoma. Invest Ophthalmol Vis Sci. 1999; 40:2627–2632. [PubMed: 10509659]
25. Sanchez RN, Chan CK, Garg S, et al. Interleukin-6 in retinal ischemia reperfusion injury in rats. Invest Ophthalmol Vis Sci. 2003; 44:4006–4011. [PubMed: 12939322]
26. Wang J, Jiang S, Kwong JM, Sanchez RN, Sadun AA, Lam TT. Nuclear factor-kappaB p65 and upregulation of interleukin-6 in retinal ischemia/reperfusion injury in rats. Brain Res. 2006; 1081:211–218. [PubMed: 16530172]
27. Niemand C, Nimmesgern A, Haan S, et al. Activation of STAT3 by IL-6 and IL-10 in primary human macrophages is differentially modulated by suppressor of cytokine signaling 3. J Immunol. 2003; 170:3263–3272. [PubMed: 12626585]
28. Bergamini A, Bolacchi F, Bongiovanni B, et al. Granulocyte-macrophage colony-stimulating factor regulates cytokine production in cultured macrophages through CD14-dependent and -independent mechanisms. Immunology. 2000; 101:254–261. [PubMed: 11012779]
29. Si Q, Nakamura Y, Ogata T, Kataoka K, Schubert P. Differential regulation of microglial activation by propentofylline via cAMP signaling. Brain Res. 1998; 812:97–104. [PubMed: 9813261]
30. Ballestas ME, Benveniste EN. Interleukin 1-beta- and tumor necrosis factor-alpha-mediated regulation of ICAM-1 gene expression in astrocytes requires protein kinase C activity. Glia. 1995; 14:267–278. [PubMed: 8530184]
31. Libermann TA, Baltimore D. Activation of interleukin-6 gene expression through the NF-kappa B transcription factor. Mol Cell Biol. 1990; 10:2327–2334. [PubMed: 2183031]
32. Alcorn JF, Wright JR. Surfactant protein A inhibits alveolar macrophage cytokine production by CD14-independent pathway. Am J Physiol. 2004; 286:L129–L136.
33. Han IO, Kim HS, Kim HC, Joe EH, Kim WK. Synergistic expression of inducible nitric oxide synthase by phorbol ester and interferon-gamma is mediated through NF-kappaB and ERK in microglial cells. J Neurosci Res. 2003; 73:659–669. [PubMed: 12929133]
34. Kuo CT, Chiang LL, Lee CN, et al. Induction of nitric oxide synthase in RAW 264.7 macrophages by lipoteichoic acid from *Staphylococcus aureus*: involvement of protein kinase C- and nuclear factor-κB-dependent mechanisms. J Biomed Sci. 2003; 10:136–145. [PubMed: 12607534]
35. Amini S, Clavo A, Nadraga Y, Giordano A, Khalili K, Sawaya BE. Interplay between cdk9 and NF-kappaB factors determines the level of HIV-1 gene transcription in astrocytic cells. Oncogene. 2002; 21:5797–5803. [PubMed: 12173051]
36. Arkan MC, Leonarduzzi G, Biasi F, Basaga H, Poli G. Physiological amounts of ascorbate potentiate phorbol ester-induced nuclear binding of AP-1 transcription factor in cells of macrophagic lineage. Free Radical Biol Med. 2001; 31:374–382. [PubMed: 11461775]
37. Contant K, Atwood WJ, Traub R, Tornatore C, Major EO. An increase in p50/p65 NF-κB binding to the HIV-1 LTR is not sufficient to increase viral expression in the primary human astrocyte. Virology. 1994; 205:586–590. [PubMed: 7975262]
38. Song J, Duncan MJ, Li G, et al. A novel TLR4-mediated signaling pathway leading to IL-6 responses in human bladder epithelial cells. PLoS Pathog. 2007; 3(4):e60. [PubMed: 17465679]

39. Kim JM, Kim JS, Lee JY, et al. Vacuolating cytotoxin in *Helicobacter pylori* water-soluble proteins upregulates chemokine expression in human eosinophils via Ca2+ influx, mitochondrial reactive oxygen intermediates, and NF-kappaB activation. Infect Immun. 2007; 75:3373–3381. [PubMed: 17452475]
40. Jeong HJ, Hong SH, Park RK, An NH, Kim HM. Ethanol induces the production of cytokines via the Ca^{2+}, MAP kinase, HIF-1alpha, and NF-kappaB pathway. Life Sci. 2005; 77:2179–2192. [PubMed: 15925386]
41. Nath A, Conant K, Chen P, Scott C, Major EO. Transient exposure to HIV-1 Tat protein results in cytokine production in macrophages and astrocytes: a hit and run phenomenon. J Biol Chem. 1999; 274:17098–17102. [PubMed: 10358063]
42. Copland IB, Post M. Stretch-activated signaling pathways responsible for early response gene expression in fetal lung epithelial cells. J Cell Physiol. 2007; 210:133–143. [PubMed: 16998809]
43. Färber K, Kettenmann H. Functional role of calcium signals for microglial function. Glia. 2006; 54:656–665. [PubMed: 17006894]
44. Kim SR, Kim SU, Oh U, Jin BK. Transient receptor potential vanilloid subtype 1 mediates microglial cell death in vivo and in vitro via Ca^{2+}-mediated mitochondrial damage and cytochrome *c* release. J Immunol. 2006; 177:4322–4329. [PubMed: 16982866]
45. Katsura H, Obata K, Mizushima T, et al. Activation of Src-family kinases in spinal microglia contributes to mechanical hypersensitivity after nerve injury. J Neurosci. 2006; 26:8680–8690. [PubMed: 16928856]
46. Inman DM, Sappington RM, Horner PJ, Calkins DJ. Quantitative correlation of optic nerve pathology with ocular pressure and corneal thickness in the DBA/2 mouse model of glaucoma. Invest Ophthalmol Vis Sci. 2006; 47:986–996. [PubMed: 16505033]
47. Bers DM. A simple method for the accurate determination of free [Ca] in Ca-EGTA solutions. Am J Physiol. 1982; 242:C404–C408. [PubMed: 6805332]
48. Otten U, Lorez HP, Businger F. Nerve growth factor antagonizes the neurotoxic action of capsaicin on primary sensory neurones. Nature. 1983; 301:515–517. [PubMed: 6185853]
49. Holzer P. Local effector functions of capsaicin-sensitive sensory nerve endings: involvement of tachykinins, calcitonin gene-related peptide and other neuropeptides. Neuroscience. 1988; 24:739–768. [PubMed: 3288903]
50. Bevan S, Szolcsányi J. Sensory neuron-specific actions of capsaicin: mechanisms and applications. Trends Pharmacol Sci. 1990; 11:330–333. [PubMed: 2203194]
51. Cereijido M, Meza I, Martinez-Palono A. Occluding junctions in cultured epithelial monolayers. Am J Physiol. 1981; 9:C96–C102. [PubMed: 7212057]
52. Galli P, Brenna A, De-Camilli P, Meldolesi S. Extracellular calcium and the organization of tight junctions in pancreatic acinar cells. Exp Cell Res. 1976; 99:178–183. [PubMed: 816663]
53. Jones JCR, Goldman AE, Steinert PM, Yuspa S, Goldman RD. Dynamic aspects of the supermolecular organization of intermediate filament networks in cultured epidermal cells. Cell Motil. 1982; 2:197–213. [PubMed: 6756644]
54. Kartenbeck J, Schmid E, Franke WW, Geiger B. Different modes of internalization of proteins associated with adherens junctions and desmosomes: experimental separation of lateral contacts induces endocytosis of desmosomal plaque material. EMBO J. 1982; 1:725–732. [PubMed: 6821357]
55. Palant CE, Duffey ME, Mookirjee BK, Ho S, Butzel CJ. Ca 2+ regulation of tight junction permeability and structure in *Necturus* gallbladder. Am J Physiol. 1981; 245:C203–C212. [PubMed: 6412561]
56. Pitelka DR, Taggart BN, Hamamoto ST. Effects of extracellular calcium depletion on membrane topography and occluding junctions of mammary cells in culture. J Cell Biol. 1983; 96:611–624.
57. Volberg T, Geiger B, Kartenbeck J, Franke WW. Changes in membrane-microfilament interaction in intercellular adherens junctions upon removal of extracellular Ca2+ ions. J Cell Biol. 1986; 102:1832–1842. [PubMed: 3084500]
58. Minta A, Kao JP, Tsien RY. Fluorescent indicators for cytosolic calcium based on rhodamine and fluorescein chromophores. J Biol Chem. 1989; 264:8171–8178. [PubMed: 2498308]

59. Lipp P, Niggli E. Ratiometric confocal Ca^{2+}-measurements with visible wavelength indicators in isolated cardiac myocytes. Cell Calcium. 1993; 14:359–372. [PubMed: 8519060]
60. Cheng H, Lederer MR, Lederer WJ, Cannell MB. Calcium sparks and [Ca^{2+}]i waves in cardiac myocytes. Am J Physiol Cell Physiol. 1996; 270:C148–C159.
61. Floto RA, Mahaut-Smith MP, Somasundaram B, Allen JM. IgG-induced Ca2+ oscillations in differentiated U937 cells a study using laser scanning confocal microscopy and co-loaded Fluo-3 and Fura-Red fluorescent probes. Cell Calcium. 1996; 18:377–389. [PubMed: 8581966]
62. Bootman M, Niggli E, Berridge M, Lipp P. Imaging the hierarchical Ca2+ signalling system in HeLa cells. J Physiol. 1997; 499:307–314. [PubMed: 9080361]
63. Perez-Terzic C, Stehno-Bittel L, Clapham DE. Nucleoplasmic and cytoplasmic differences in the fluorescence properties of the calcium indicator Fluo-3. Cell Calcium. 1997; 21:275–282. [PubMed: 9160163]
64. Gee KR, Brown KA, Chen WN, Bishop-Stewart J, Gray D, Johnson I. Chemical and physiological characterization of fluo-4 Ca(2+)-indicator dyes. Cell Calcium. 2000; 27:97–106. [PubMed: 10756976]
65. Harvey DM, Calkins DJ. Localization of kainate receptors to the presynaptic active zone of the rod photoreceptor in primate retina. Vis Neurosci. 2002; 19:681–692. [PubMed: 12507334]
66. Calkins DJ, Sappington RM, Hendry SH. Morphological identification of ganglion cells expressing the alpha subunit of type II calmodulin-dependent protein kinase in the macaque retina. J Comp Neurol. 2005; 481:194–209. [PubMed: 15562509]
67. Chang B, Smith RS, Hawes NL, et al. Interacting loci cause severe iris atrophy and glaucoma in DBA/2J mice. Nat Genet. 1999; 21:405–409. [PubMed: 10192392]
68. John SW, Smith RS, Savinova OV, et al. Essential iris atrophy, pigment dispersion, and glaucoma in DBA/2J mice. Invest Ophthalmol Vis Sci. 1998; 39:951–962. [PubMed: 9579474]
69. Pessah IN, Waterhouse AL, Casida JE. The calcium-ryanodine receptor complex of skeletal and cardiac muscle. Biochem Biophys Res Commun. 1985; 128:449–456. [PubMed: 3985981]
70. Pessah IN, Francini AO, Scales DJ, Waterhouse AL, Casida JE. Calcium-ryanodine receptor complex: solubilization and partial characterization from skeletal muscle junctional sarcoplasmic reticulum vesicles. J Biol Chem. 1986; 261:8643–8648. [PubMed: 3722165]
71. Maggi CA, Patacchini R, Santicioli P, Giuliani S, Geppetti P, Meli A. Protective action of ruthenium red toward capsaicin desensitization of sensory fibers. Neurosci Lett. 1988; 88:201–205. [PubMed: 2454437]
72. Maggi CA, Santicioli P, Geppetti P, et al. The antagonism induced by ruthenium red of the actions of capsaicin on the peripheral terminals of sensory neurons: further studies. Eur J Pharmacol. 1988; 154:1–10. [PubMed: 2460362]
73. Wood JN, Winter J, James IF, Rang HP, Yeats J, Bevan S. Capsaicin-induced ion fluxes in dorsal root ganglion cells in culture. J Neurosci. 1988; 8:3208–3220. [PubMed: 3171675]
74. Amann R, Lembeck F. Ruthenium red selectively prevents capsaicin-induced nociceptor stimulation. Eur J Pharmacol. 1989; 161:227–229. [PubMed: 2470598]
75. Amann R, Donnerer J, Lembeck F. Capsaicin-induced stimulation of polymodal nociceptors is antagonized by ruthenium red independently of extracellular calcium. Neuroscience. 1989; 32:255–259. [PubMed: 2479880]
76. Chahl LA. The effects of ruthenium red on the response of guinea-pig ileum to capsaicin. Eur J Pharmacol. 1989; 169:241–247. [PubMed: 2478375]
77. Klegeris A, Choi HB, McLarnon JG, McGeer PL. Functional ryanodine receptors are expressed by human microglia and THP-1 cells: their possible involvement in modulation of neurotoxicity. J Neurosci Res. 2007; 85:2207–2215. [PubMed: 17526017]
78. Ma J, Pan Z. Retrograde activation of store-operated calcium channel. Cell Calcium. 2003; 33:375–384. [PubMed: 12765683]
79. Bardo S, Cavazzini MG, Emptage N. The role of the endoplasmic reticulum Ca^{2+} store in the plasticity of central neurons. Trends Pharmacol Sci. 2006; 27:78–84. [PubMed: 16412523]
80. Kollarik M, Undem BJ. Mechanisms of acid-induced activation of airway afferent nerve fibres in guinea-pig. J Physiol. 2002; 543(pt 2):591–600. [PubMed: 12205192]

81. Undem BJ, Kollarik M. Characterization of the vanilloid receptor 1 antagonist iodo-resiniferatoxin on the afferent and efferent function of vagal sensory C-fibers. J Pharmacol Exp Ther. 2002; 303:716–722. [PubMed: 12388656]
82. Seabrook GR, Sutton KG, Jarolimek W, et al. Functional properties of the high-affinity TRPV1 (VR1) vanilloid receptor antagonist (4-hydroxy-5-iodo-3-methoxyphenylacetate ester) iodo-resiniferatoxin. J Pharmacol Exp Ther. 2002; 303:1052–1060. [PubMed: 12438527]
83. Rigoni M, Trevisani M, Gazzieri D, et al. Neurogenic responses mediated by vanilloid receptor-1 (TRPV1) are blocked by the high affinity antagonist, iodo-resiniferatoxin. Br J Pharmacol. 2003; 138:977–985. [PubMed: 12642400]
84. Lou YP, Franco-Cereceda A, Lundberg JM. Different ion channel mechanisms between low concentrations of capsaicin and high concentrations of capsaicin and nicotine regarding peptide release from pulmonary afferents. Acta Physiol Scand. 1992; 146:119–127. [PubMed: 1279940]
85. Walpole CS, Wrigglesworth R, Bevan S, et al. Analogues of capsaicin with agonist activity as novel analgesic agents; structure-activity studies, 2: the amide bond “B-region”. J Med Chem. 1993; 36:2373–2380. [PubMed: 8360882]
86. Kusano K, Gainer H. Modulation of voltage-activated Ca currents by pain-inducing agents in a dorsal root ganglion neuronal line, F-11. J Neurosci Res. 1993; 34:158–169. [PubMed: 8383774]
87. Bowie D, Feltz P, Schlichter R. Subpopulations of neonatal rat sensory neurons express functional neurotransmitter receptors which elevate intracellular calcium. Neuroscience. 1994; 58:141–149. [PubMed: 7512702]
88. Fox AJ, Urban L, Barnes PJ, Dray A. Effects of capsazepine against capsaicin- and proton-evoked excitation of single airway C-fibres and vagus nerve from the guinea-pig. Neuroscience. 1995; 67:741–752. [PubMed: 7675200]
89. Liu M, Liu MC, Magoulas C, Priestley JAV, Willmott NJ. Versatile regulation of cytosolic Ca^{2+} by vanilloid receptor-1 in rat dorsal root ganglion neurons. J Biol Chem. 2003; 278:5462–5472. [PubMed: 12454015]
90. Marshall ICB, Owen DE, Cripps TV, Davis JB, McNulty S, Smart D. Activation of vanilloid receptor 1 by resiniferatoxin mobilizes calcium from inositol 1,4,5-triphosphate-sensitive stores. Br J Pharmacol. 2003; 138:172–176. [PubMed: 12522087]
91. Imagawa T, Smith JS, Coronado R, Campbell KP. Purified ryanodine receptor from skeletal muscle sarcoplasmic reticulum is the Ca2+-permeable pore of the calcium release channel. J Biol Chem. 1987; 262:16636–16643. [PubMed: 2445748]
92. Damiani E, Margreth A. Characterization study of the ryanodine receptor and of calsequestrin isoforms of mammalian skeletal muscles in relation to fibre types. J Muscle Res Cell Motil. 1994; 15:86–101. [PubMed: 8051290]
93. Carr MJ, Kollarik M, Meeker SN, Undem BJ. A role for TRPV1 in bradykinin-induced excitation of vagal airway afferent nerve terminals. J Pharmacol Exp Ther. 2003; 304:1275–1279. [PubMed: 12604706]
94. Fischer MJ, Reeh PW, Sauer SK. Proton-induced calcitonin gene-related peptide release from rat sciatic nerve axons, in vitro, involving TRPV1. Eur J Neurosci. 2003; 18:803–810. [PubMed: 12925006]
95. Pethö G, Izydorczyk I, Reeh PW. Effects of TRPV1 receptor antagonists on stimulated iCGRP release from isolated skin of rats and TRPV1 mutant mice. Pain. 2004; 109:284–290. [PubMed: 15157689]
96. Lu G, Henderson D, Liu L, Reinhart PH, Simon SA. TRPV1b, a functional human vanilloid receptor splice variant. Mol Pharmacol. 2005; 67:1119–1127. [PubMed: 15644492]
97. Veronesi B, Carter JD, Devlin RB, Simon SA, Oortgiesen M. Neuropeptides and capsaicin stimulate the release of inflammatory cytokines in a human bronchial epithelial cell line. Neuropeptides. 1999; 33:447–456. [PubMed: 10657523]
98. Southall MD, Li T, Gharibova LS, Pei Y, Nicol GD, Travers JB. Activation of epidermal vanilloid receptor-1 induces release of proinflammatory mediators in human keratinocytes. J Pharmacol Exp Ther. 2003; 304:217–222. [PubMed: 12490594]

99. Zhang F, Yang H, Wang Z, et al. Transient receptor potential vanilloid 1 activation induces inflammatory cytokine release in corneal epithelium through MAPK signaling. J Cell Physiol. 2007; 213:730–739. [PubMed: 17508360]
100. Yoon J, Ben-Ami HC, Hong YS, et al. Novel mechanism of massive photoreceptor degeneration caused by mutations in trp gene of *Drosophila*. J Neurosci. 2000; 20:649–659. [PubMed: 10632594]
101. Hong YS, Park S, Geng C, et al. Single amino acid change in the fifth transmembrane segment of the TRP Ca^{2+} channel causes massive degeneration of photoreceptors. J Biol Chem. 2002; 277:33884–33889. [PubMed: 12107168]
102. Corey DP. New TRP channels in hearing and mechanosensation. Neuron. 2003; 39:585–588. [PubMed: 12925273]
103. Rigoni M, Trevisani M, Gazzieri D, et al. Neurogenic responses mediated by vanilloid receptor-1 (TRPV1) are blocked by the high affinity antagonist, iodo-resiniferatoxin. Br J Pharmacol. 2003; 138:977–985. [PubMed: 12642400]
104. Agopyan N, Bhatti T, Yu S, Simon SA. Vanilloid receptor activation by 2- and 10-mm particles induces responses leading to apoptosis in human airway epithelial cells. Toxicol Appl Pharm. 2003; 192:21–35.
105. Corey DP, Garcia-Anoveros J, Holt JR, et al. TRPA1 is a candidate for the mechanosensitive transduction channel of vertebrate hair cells. Nature. 2004; 432:723–730. [PubMed: 15483558]
106. Puntambekar P, Van Buren J, Raisinghani M, Premkumar LS, Ramkumar V. Direct interaction of adenosine with the TRPV1 channel protein. J Neurosci. 2004; 24:3663–3671. [PubMed: 15071115]
107. Lakshmi S, Joshi PG. Co-activation of P2Y2 receptor and TRPV channel by ATP: implications for ATP induced pain. Cell Mol Neurobiol. 2005; 25:819–832. [PubMed: 16133936]
108. van der Stelt M, Trevisani M, Vellani V, et al. Anandamide acts as an intracellular messenger amplifying Ca2+ influx via TRPV1 channels. EMBO J. 2005; 24:3026–3037. [PubMed: 16107881]
109. El Kouhen R, Surowy CS, Bianchi BR, et al. A-425619 [1-isoquinolin-5-yl-3-(4-trifluoromethyl-benzyl)-urea], a novel and selective transient receptor potential type V1 receptor antagonist, blocks channel activation by vanilloids, heat, and acid. J Pharmacol Exp Ther. 2005; 314:400–409. [PubMed: 15837819]
110. Toth A, Wang Y, Kedei N, et al. Different vanilloid agonists cause different patterns of calcium response in CHO cells heterologously expressing rat TRPV1. Life Sci. 2005; 76:2921–2932. [PubMed: 15820503]
111. Reilly CA, Johansen ME, Lanza DL, Lee J, Lim JO, Yost GS. Calcium-dependent and independent mechanisms of capsaicin receptor (TRPV1)-mediated cytokine production and cell death in human bronchial epithelial cells. J Biochem Mol Toxicol. 2005; 19:266–275. [PubMed: 16173059]
112. Naskar R, Wissing M, Thanos S. Detection of early neuron degeneration and accompanying microglial responses in the retina of a rat model of glaucoma. Invest Ophthalmol Vis Sci. 2002; 43:2962–2968. [PubMed: 12202516]
113. Ju KR, Kim HS, Kim JH, Lee NY, Park CK. Retinal glial cell responses and Fas/FasL activation in rats with chronic ocular hypertension. Brain Res. 2006; 1122:209–221. [PubMed: 17045251]
114. Eun SY, Jung SJ, Park YK, Kwak J, Kim SJ, Kim J. Effects of capsaicin on Ca^{2+} release from the intracellular Ca(2+) stores in the dorsal root ganglion cells of adult rats. Biochem Biophys Res Commun. 2001; 285:1114–1120. [PubMed: 11478769]
115. Tabibzadeh SS, Santhanam U, Sehgal PB, May LT. Cytokine-induced production of IFN-beta 2/IL-6 by freshly explanted human endometrial stromal cells: modulation by estradiol-17 beta. J Immunol. 1989; 142:3134–3139. [PubMed: 2651521]
116. Brown TD. Techniques for mechanical stimulation of cells in vitro: a review. J Biomech. 2000; 33:3–14. [PubMed: 10609513]
117. Hernandez MR, Pena JDO, Selvidge JA, Salvador-Silva M, Yang P. Hydrostatic pressure stimulates synthesis of elastin in cultured optic nerve head astrocytes. Glia. 2000; 32:122–136. [PubMed: 11008212]

118. Tanck E, van Driel WD, Hagen JW, Burger EH, Blankevoort L, Huiskes R. Why does intermittent hydrostatic pressure enhance the mineralization process in fetal cartilage? J Biomech. 1999; 32:153–161. [PubMed: 10052920]

119. Kaarniranta K, Elo M, Sironen R, et al. Hsp70 accumulation in chondrocytic cells exposed to high continuous hydrostatic pressure coincides with mRNA stabilization rather than transcriptional activation. Proc Natl Acad Sci USA. 1998; 95:2319–2324. [PubMed: 9482883]

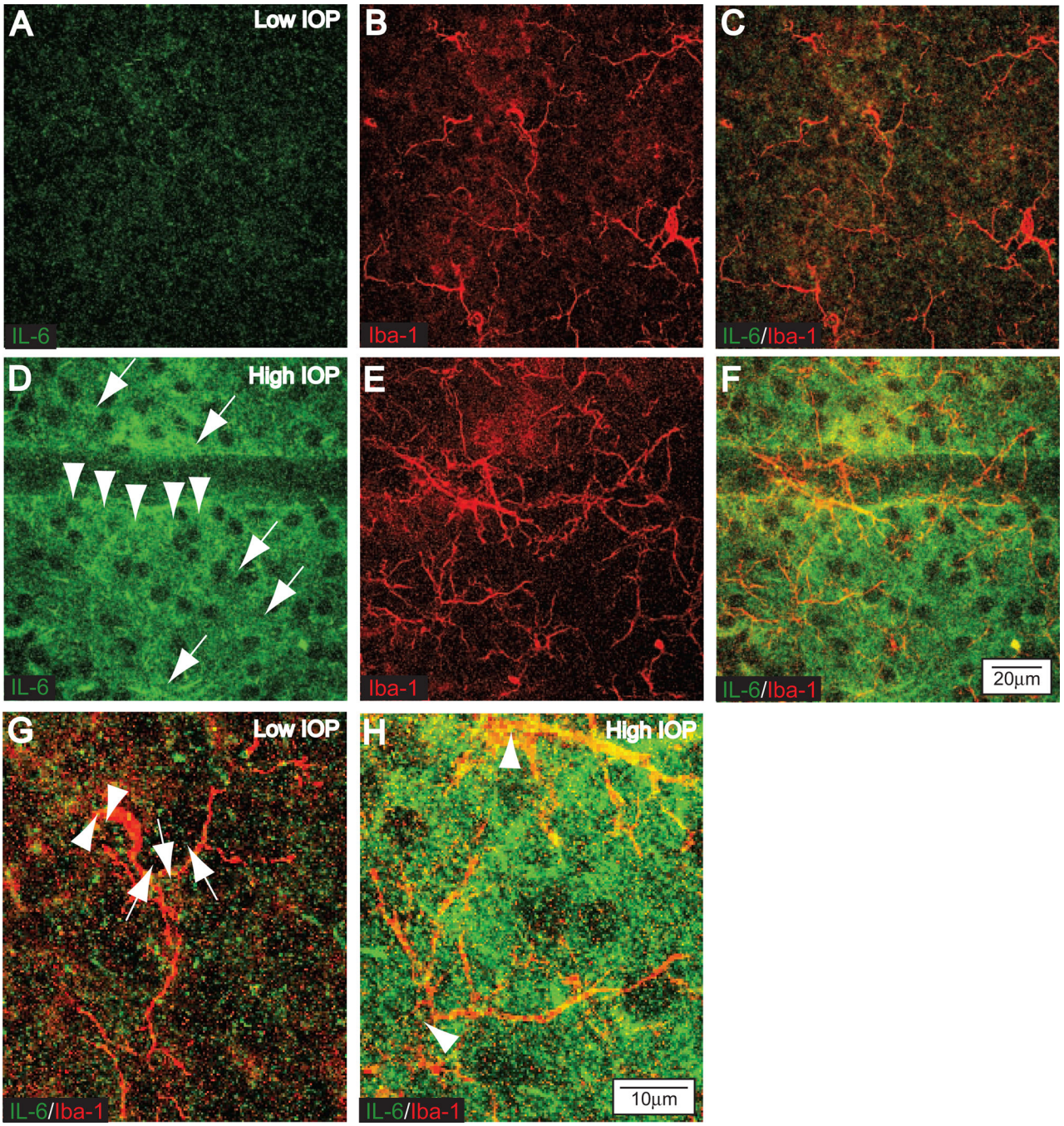

Figure 1.

IL-6 Increases with elevated IOP in the DBA/2 mouse model of glaucoma. Confocal micrographs through the ganglion cell layer of 6-month-old DBA/2 retinas immuno-labeled for IL-6 and the microglia-specific marker Iba-1. Retina from eyes with relatively low IOP (average, 14.7 mm Hg; **A–C**) or higher IOP (average, 21.2 mm Hg; **D–F**). (**A**) Modest level of extracellular IL-6 in the ganglion cell layer of a retina with low IOP. (**B**) Several microglia in the same focal plane labeled by Iba-1. (**C**) Overlay of IL-6 and Iba1 reveals a low level of colocalization (*yellow*) associated mainly with microglial processes. (**D**)

Stronger IL-6 labeling in retina with elevated IOP is concentrated in the extracellular space surrounding RGC cell bodies (*arrows*) and in cellular processes near RGCs (*arrowheads*). (**E**) Iba-1 labeling in the same field reveals hypertrophic microglial processes and an increase in ramification (compare with **B**). (**F**) Overlay reveals increased colocalization (*yellow*) of IL-6 and Iba-1, primarily in the processes of microglia. Scale is the same for (**A–F**). (**G**) Higher magnification of Iba-1 and IL-6 labeling shown in (**C**) demonstrates colocalization in microglia cell bodies (*arrowheads*) and processes (*arrows*). (**H**) Higher magnification of (**F**) reveals even stronger colocalization with increased IOP. Microglia cell bodies are indicated (*arrowheads*). Scale is the same for (**G, H**).

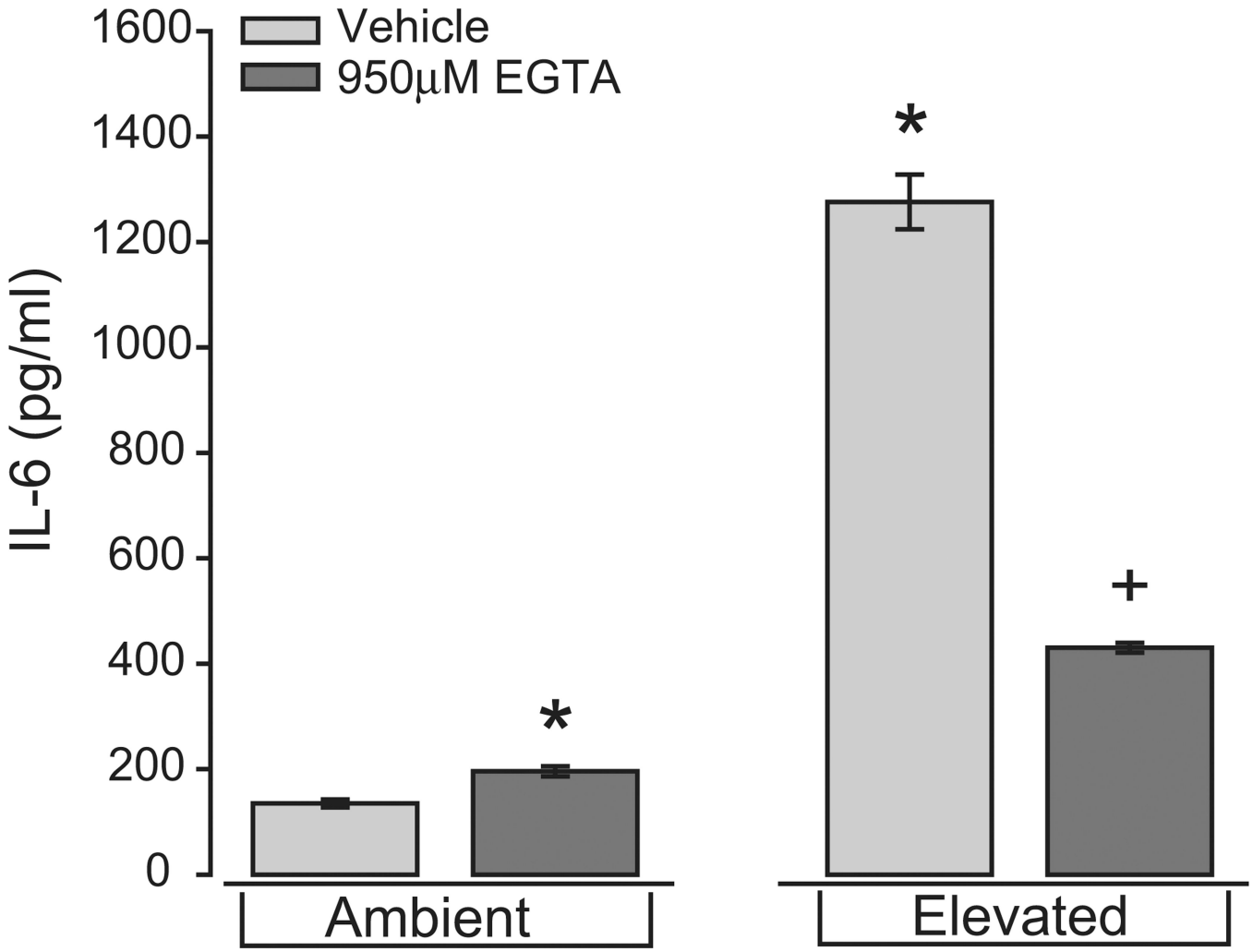

Figure 2.

Chelation of extracellular Ca^{2+} inhibits pressure-induced IL-6 release by retinal microglia. ELISA measurements of IL-6 concentration in the culture media of primary retinal microglia exposed to ambient or elevated pressure for 24 hours in the presence or absence of the Ca^{2+} chelator EGTA (950 μM). $^{*}P \leq 0.05$ compared with ambient pressure alone. $^{+}P < 0.05$ compared with elevated pressure alone. $n = 4$ per condition.

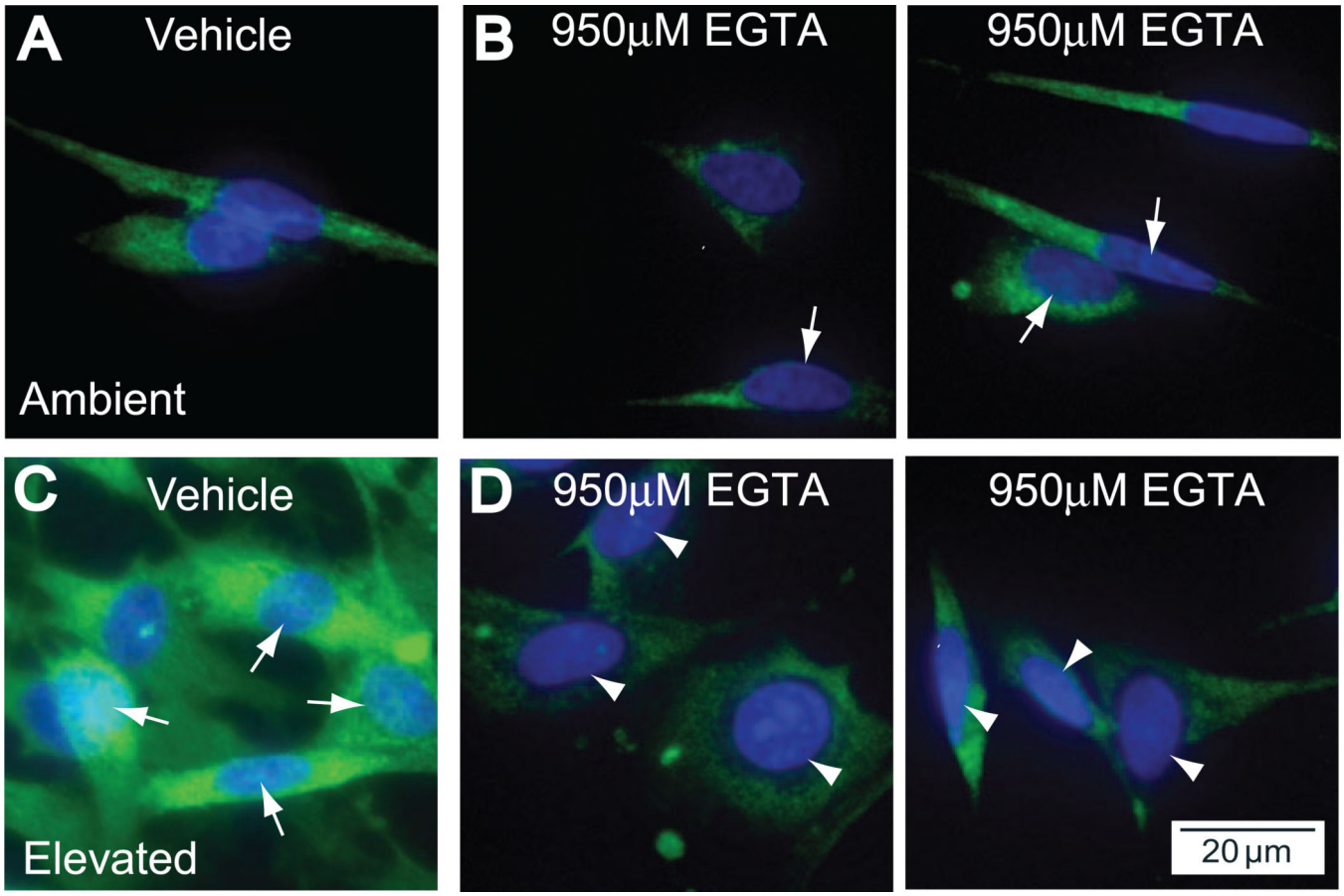

Figure 3.

Chelation of extracellular Ca^{2+} inhibits the translocation of NFκB in retinal microglia. Primary cultures of retinal microglia exposed to ambient or elevated pressure for 24 hours alone (**A, C**) or with the Ca^{2+} chelator EGTA (950 μM; **B, D**). (**A**) Fluoromicrograph of immunolabeling against the p65 subunit of NFκB (*green*) with nuclear counterstain DAPI (*blue*) at ambient pressure. With EGTA treatment (**B**), there is a very slight increased incidence of colocalization of NFκB with DAPI (*arrows*). (**C**) Elevated pressure induces increased cytosolic NFκB and nuclear translocation, as seen by strong colocalization with DAPI (*arrows*). (**D**) Treatment with EGTA reduces cytosolic NFκB and nuclear translocation, as seen by decreased colocalization with DAPI (*arrowheads*).

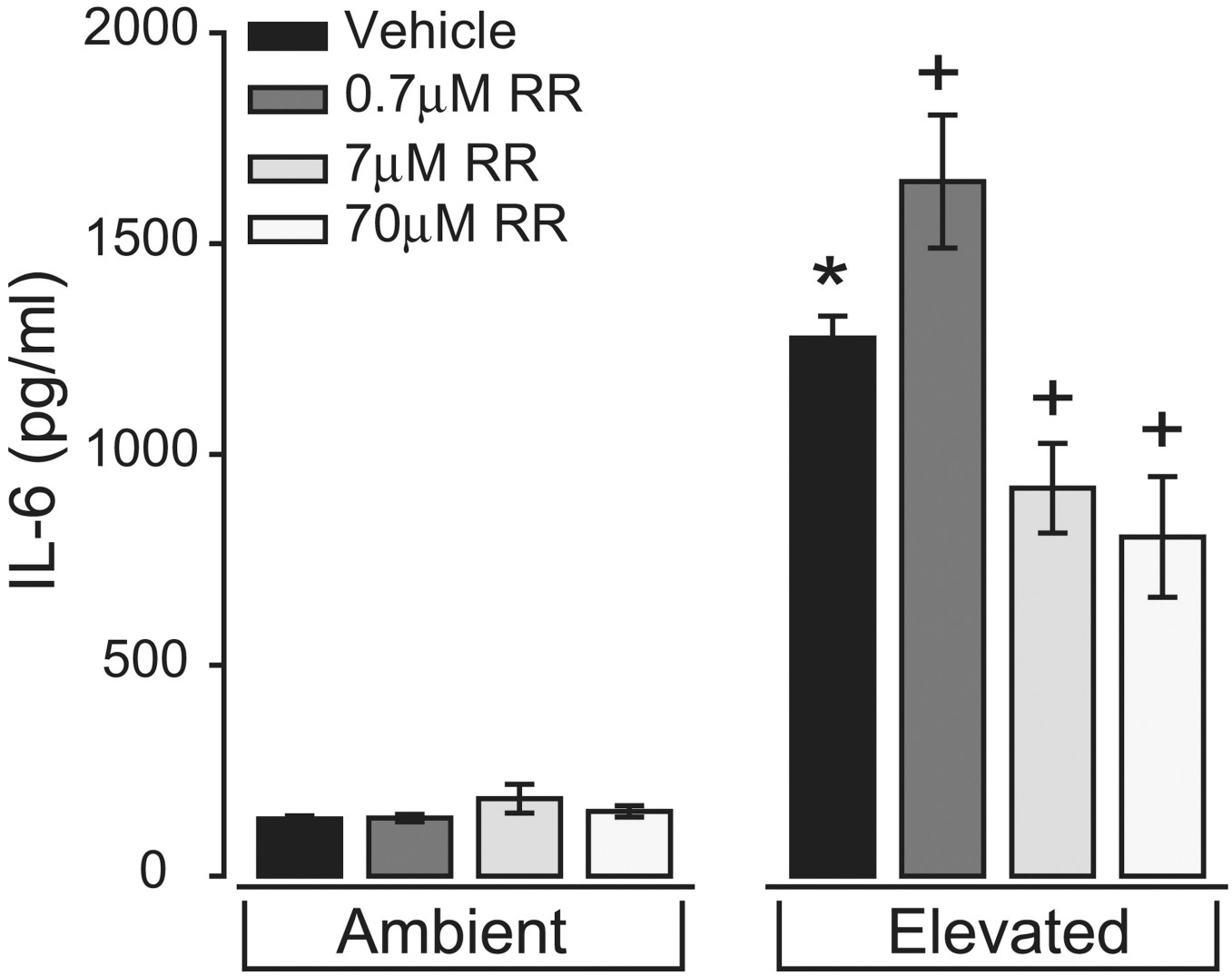

Figure 4.

Treatment with ruthenium red inhibits pressure-induced IL-6 release in retinal microglia. ELISA measurements of the IL-6 in culture media of primary retinal microglia exposed to ambient (*left*) or elevated (*right*) pressure for 24 hours in the presence or absence of the broad-spectrum Ca^{2+} channel inhibitor ruthenium red (RR; 0.7–70 μM). $^{*}P \leq 0.05$ compared with ambient pressure alone. $^{+}P \leq 0.05$ compared with elevated pressure alone. $n = 3$ per condition.

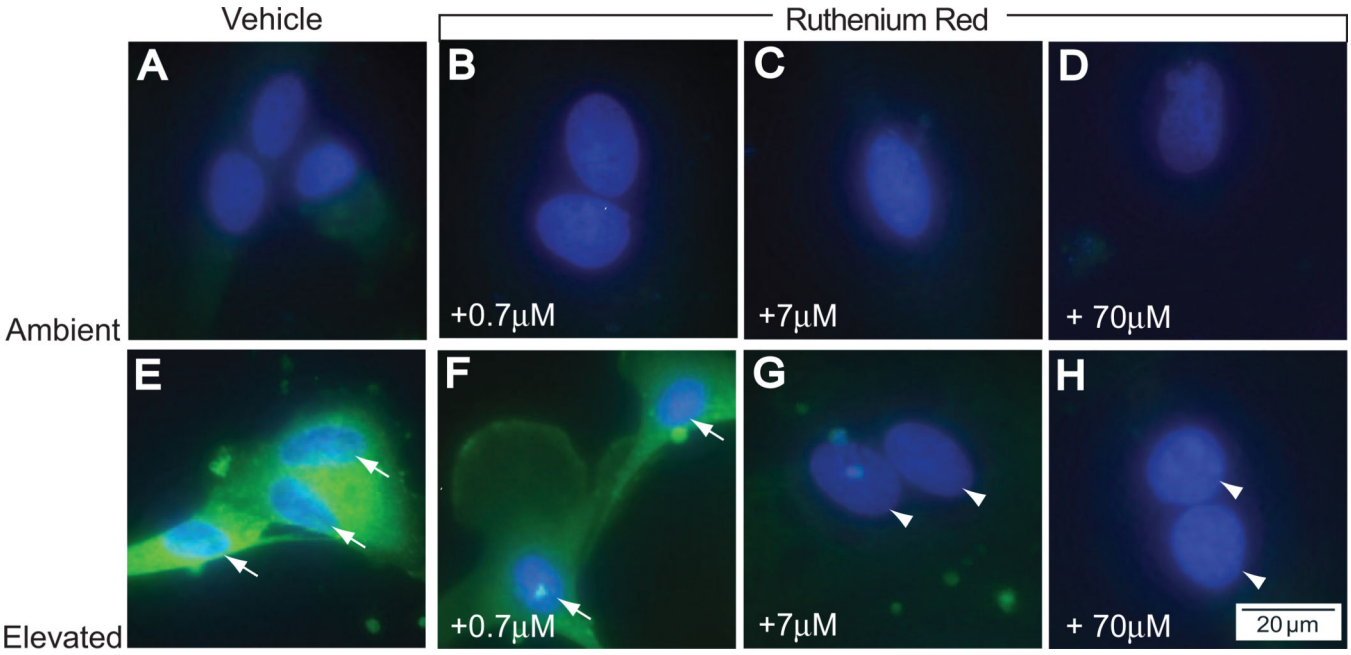

Figure 5.

Treatment with ruthenium red inhibits pressure-induced translocation of NFκB in retinal microglia. Primary cultures of retinal microglia exposed to ambient (**A–D**) or elevated (**E–H**) pressure for 24 hours in the presence or absence of ruthenium red. (**A**) Fluoromicrograph of immunolabeling against the p65 subunit of NFκB (*green*) with nuclear counterstain DAPI (*blue*) at ambient pressure. Treatment with increasing concentrations of ruthenium red (**B–D**) does not alter levels of cytosolic NFκB or nuclear translocation. (**E**) Elevated pressure induces increased cytosolic NFκB and nuclear translocation, as seen by colocalization of NFκB and DAPI (*arrows*). Treatment with 0.7 μM ruthenium red (**F**) alters NFκB translocation very little, but treatment with 7 μM (**G**) and 70 μM ruthenium red (**H**) dramatically reduces cytosolic NFκB and nuclear translocation (*arrowheads*).

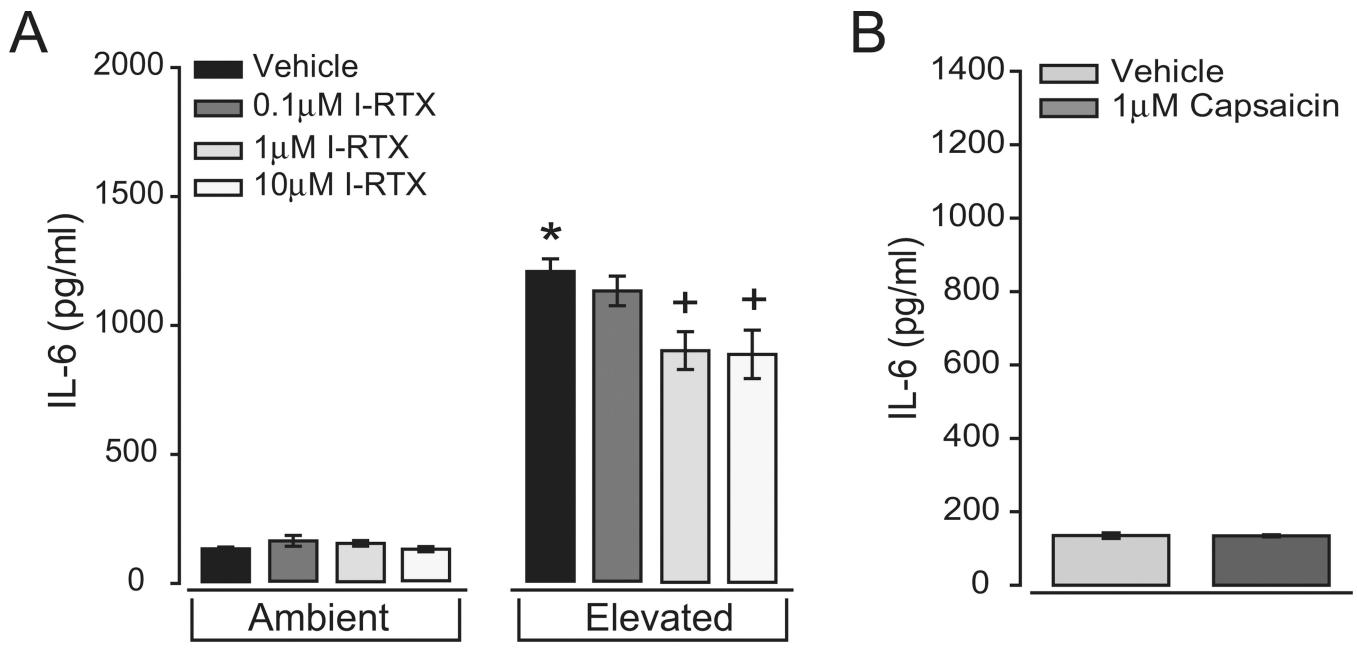

Figure 6.

Antagonism of TRPV1 inhibits pressure-induced IL-6 release in retinal microglia. (**A**) ELISA measurements of IL-6 concentration in the culture media of primary retinal microglia exposed to ambient (*left*) or elevated (*right*) pressure for 24 hours in the presence or absence of the TRPV1-specific antagonist iodo-resiniferatoxin (I-RTX; 0.1–10 μM). (**B**) ELISA measurements of IL-6 concentration in the media of primary microglia cultures maintained at ambient pressure in the presence or absence of 1 μM capsaicin for 24 hours. $^{*}P < 0.05$ compared with ambient pressure alone. $^{+}P \leq 0.05$ compared with elevated pressure alone. $n = 3$ per condition.

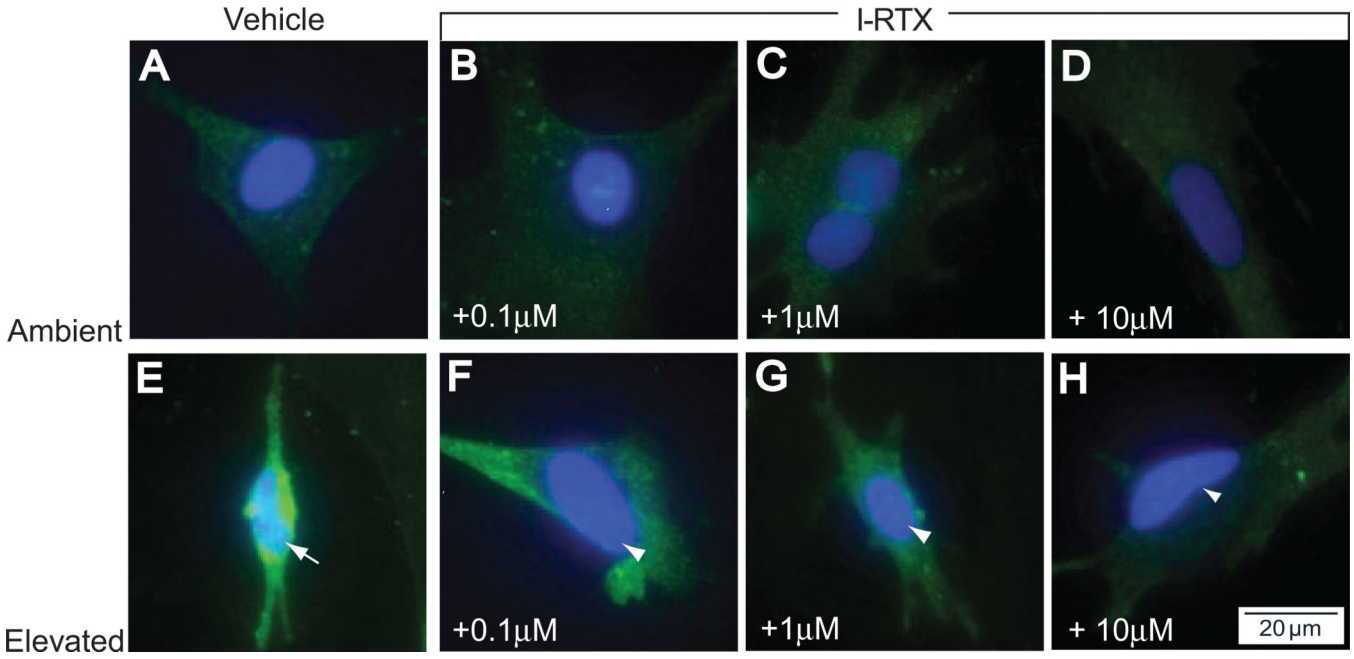

Figure 7.

Antagonism of TRPV1 inhibits pressure-induced translocation of NFκB in retinal microglia. Microglia exposed to ambient or elevated pressure for 24 hours with the TRPV1-specific antagonist I-RTX (0.1–10 μM) and immunolabeled for NFκB (*green*) and counterstained with DAPI (*blue*). At ambient pressure, increasing concentrations of I-RTX have little effect on either NFκB levels or translocation (compare **A** with **B–D**). At elevated pressure, increased cytosolic NFκB and translocation, shown by colocalization of NFκB and DAPI (**E**, *arrows*), are inhibited by treatment with I-RTX (*arrowheads*; **F–H**).

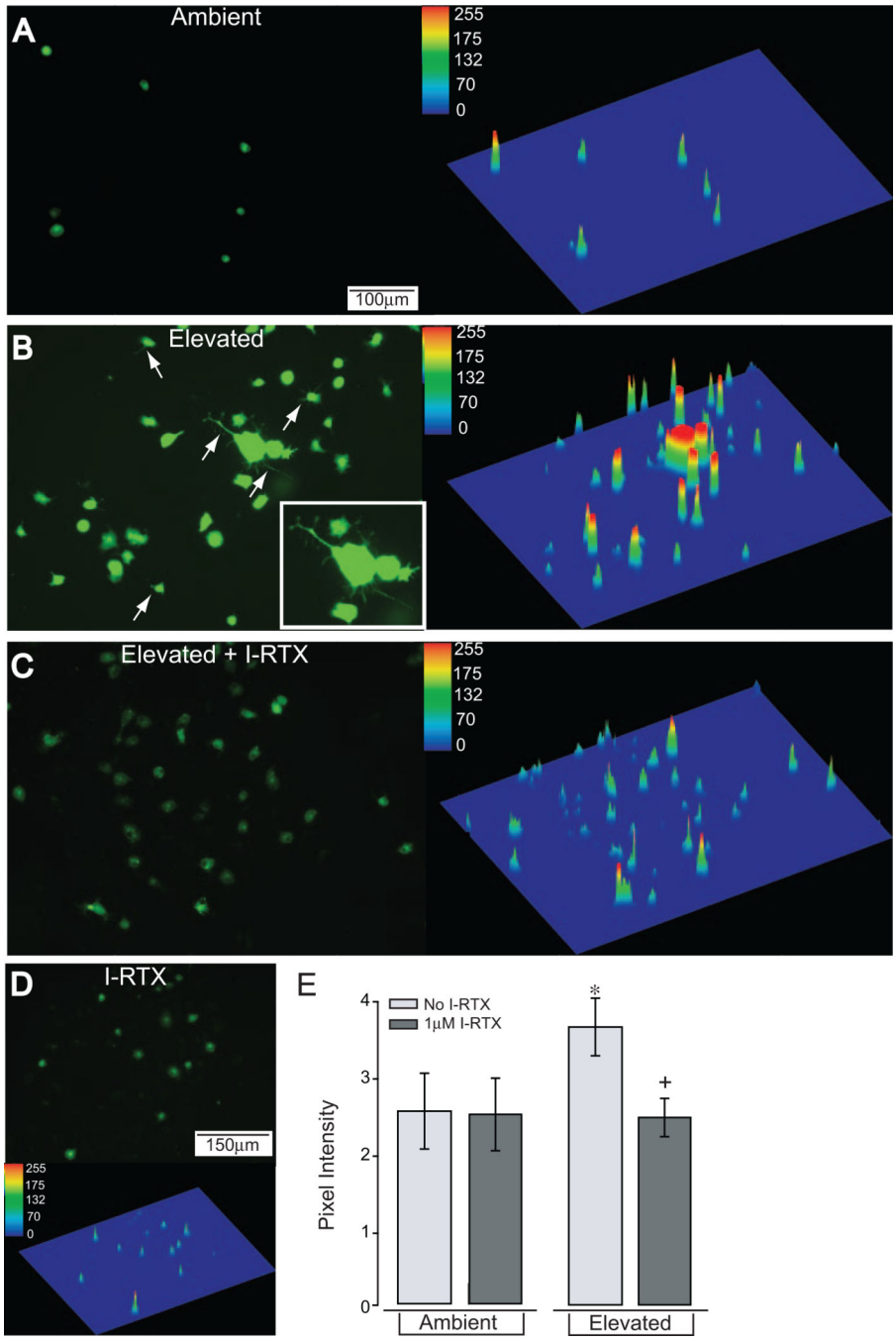

Figure 8.

Antagonism of TRPV1 attenuates pressure-induced increases in microglia Ca^{2+} levels. Fluoromicrographs with corresponding surface plots of primary cultures of retinal microglia exposed to ambient or elevated pressure for 1 hour after incubation with the Ca^{2+} dye Fluo-4 AM. (**A**) Fluo-4 label is present at very low levels in microglia maintained at ambient pressure (*left*). A plot of signal distribution reveals Fluo-4 label in what are most likely cell bodies (*right*). (**B**) Elevated pressure qualitatively increases Fluo-4 intensity (*right*) and induces Fluo-4 label in microglial processes (*arrows* and *inset*; *left*). (**C**) Treatment with I-

RTX qualitatively reduces Fluo-4 label in cell bodies and processes (compare **C** and **B**). (**D**) Treatment with I-RTX at ambient pressure does not appear to alter Fluo-4 labeling (compare **D** and **A**). Scale is the same for (**A**–**D**). (**E**) Quantification of Fluo-4 label indicates a 54% increase in intensity for microglia exposed to elevated pressure (*). I-RTX treatment reversed this pressure-induced increase in Fluo-4 intensity ($^{+}$). Symbols indicate $P \leq 0.05$; error bars represent SE. Pixel intensity was calculated as the average of total intensity from 15 to 20 independent fields. $n = 3$ per condition.

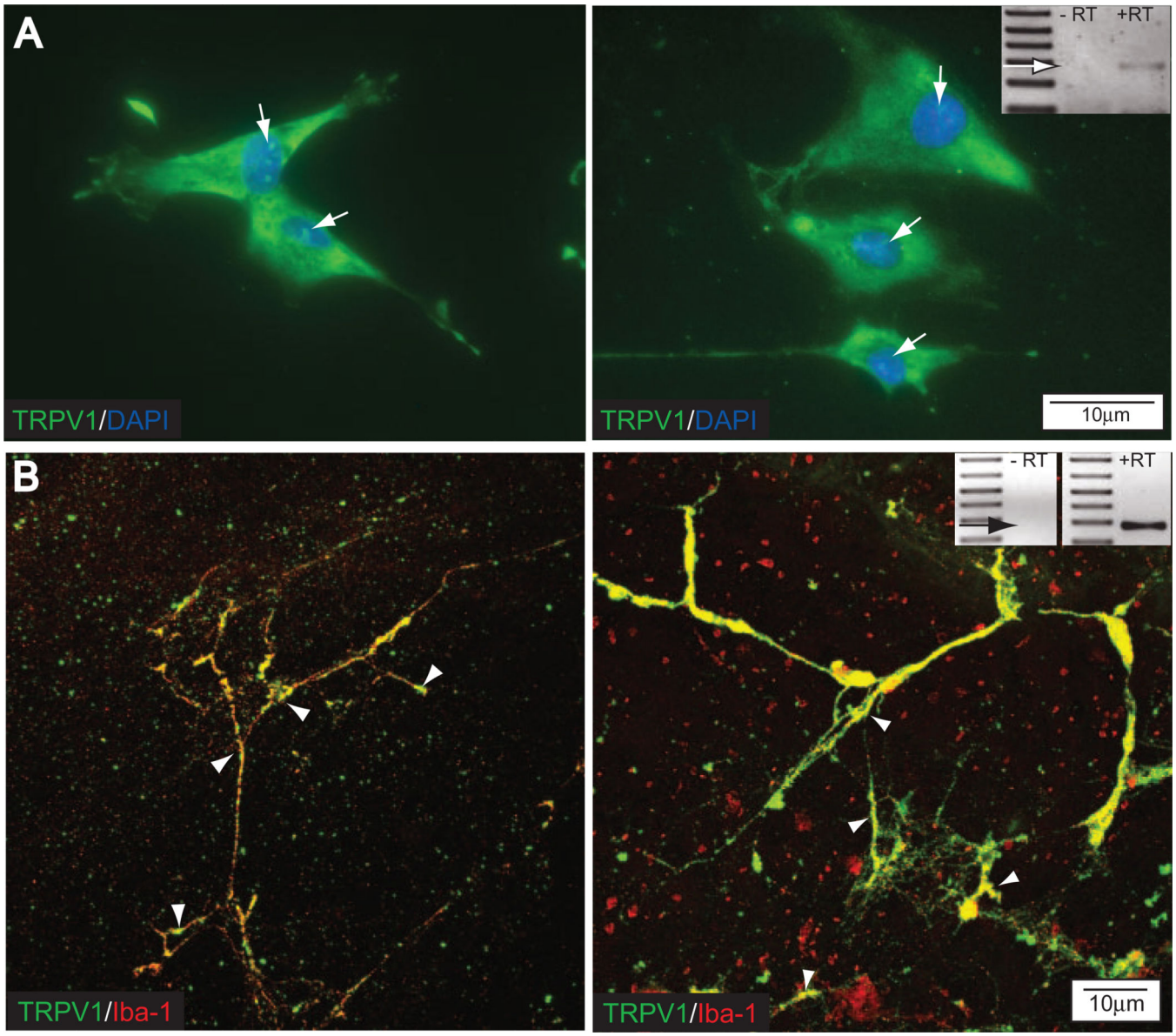

Figure 9.

Retinal microglia express TRPV1 in vitro and in vivo. (**A**) Fluoromicrograph of TRPV1 immunolabel (*green*) with DAPI counterstain (*blue*) in primary cultures of retinal microglia. Diffuse distribution and perinuclear labeling (*arrows*) suggest TRPV1 localization to the endoplasmic reticulum and the plasma membrane. (*inset*) PCR product for TRPV1 in a RNA sample from primary cultures of retinal microglia (+RT). Control sample (−RT) is the same sample without reverse transcription. (**B**) Confocal micrograph of coimmunolabeling against TRPV1 (*green*) and the microglia-specific marker Iba-1 (*red*) in a whole mount preparation of retina from adult rat. Colocalization of Iba-1 and TRPV1 (*yellow*) confirms the expression of TRPV1 by microglia. Punctate labeling for TRPV1 in the processes suggests localization to the plasma membrane (*arrowheads*), whereas more diffuse labeling in the cell body suggests localization to the endoplasmic reticulum. Plane of focus is at the border of the nerve fiber and ganglion cell layers. *Inset*: PCR product for TRPV1 in an RNA sample

from whole retina of adult rat (+RT). Control sample (−RT) is the same sample without reverse transcription.